NASA Technical Paper 1888

Aerodynamic Tests and Analysis of a Turbojet-Boosted Launch Vehicle Concept (Spacejet) Over a Mach Number Range of 1.50 to 2.86

Gregory D. Riebe, William J. Small,
and Odell A. Morris

JULY 1981

NASA

NASA Technical Paper 1888

Aerodynamic Tests and Analysis of a Turbojet-Boosted Launch Vehicle Concept (Spacejet) Over a Mach Number Range of 1.50 to 2.86

Gregory D. Riebe, William J. Small,
and Odell A. Morris
Langley Research Center
Hampton, Virginia

NASA
National Aeronautics
and Space Administration

**Scientific and Technical
Information Branch**

1981

SUMMARY

Results from analytical and experimental studies of the aerodynamic characteristics of a turbojet-boosted launch vehicle concept through a Mach number range of 1.50 to 2.86 are presented. The vehicle consists of a winged orbiter utilizing an area-ruled axisymmetric body and two winged turbojet boosters mounted underneath the orbiter wing. This study concentrated primarily on drag characteristics near zero lift. Force measurements and flow visualization techniques were employed. Estimates from wave drag theory, supersonic lifting surface theory, and impact theory are compared with data and indicate the ability of these theories to adequately predict the aerodynamic characteristics of the vehicle. Despite the existence of multiple wings and bodies in close proximity to each other, no large scale effects of boundary-layer separation on drag or lift could be discerned. Total drag levels were, however, sensitive to booster locations.

INTRODUCTION

Various studies have been made in an effort to identify key requirements and problems of possible second-generation space transportation systems. Several concepts have been put forth as offering solutions to perceived future needs. (See refs. 1 to 5.) This paper will address the supersonic aerodynamics of one of these concepts, a turbojet-boosted orbiter referred to as the Spacejet. (See refs. 3 and 5.)

Key features of the Spacejet concept are illustrated in figure 1. The system is completely reusable and would operate from runways in a manner much like conventional aircraft. A rocket-powered orbiter containing liquid hydrogen and oxygen propellants is supported by twin boosters during take-off. These boosters each have six to eight large hydrocarbon-fueled turbojet engines of the type proposed for future supersonic transports. The boosters contain their own fuel and the heavy take-off rolling gear which can typically weigh as much as the orbiter payload (29 500 kg (65 000 lb)). At take-off rotation, lift forces of nearly 580 000 N (2.6×10^6 lb) must be generated by the complete vehicle, including orbiter and booster lifting surfaces and any lift component of booster thrust. After a high angle-of-attack take-off, the vehicle accelerates on turbojet thrust to a staging Mach number near 3.5. During acceleration to this staging Mach number, a high dynamic-pressure trajectory is followed to maximize thrust of the turbojet engines minus vehicle drag. At staging, both boosters separate and fly back to base. At the same time, rocket engines are ignited which propel the orbiter into Earth orbit. Reentry and landing of the orbiter are similar to present space shuttle operation.

Preliminary design studies of the Spacejet concept indicated vehicle area ruling was theoretically of great importance in reducing transonic wave drag (ref. 6). The full-scale concept, therefore, was area ruled to optimize the

complete vehicle wave drag at Mach 1.3. The geometrical complexity of the concept, however, gave rise to concerns that flow separation caused by interaction effects between wings and bodies could drastically increase drag above the theoretically calculated values. Accordingly, a 1/100-scale wind-tunnel-model representation of the full-scale concept was built to test the validity of theoretical methods for this class of configurations. This paper presents the results of the high-speed (Mach 1.50 to 2.86) wind-tunnel investigation of this model. A general overview of the aerodynamics of the Spacejet across the Mach number range from 0.3 to 2.86 is presented in reference 6.

SYMBOLS

The longitudinal characteristics are presented about the stability-axis system. The moment reference point was at a longitudinal station 75.0 percent of the fuselage length aft of the nose. Measurements and calculations were made in the U.S. Customary Units. They are presented herein in the International System of Units (SI) and parenthetically in U.S. Customary Units. For a description of model nomenclature, see the appendix.

C_D drag coefficient, $\text{Drag}/q_\infty S_{ref}$

$C_{D,min}$ minimum drag coefficient

C_L lift coefficient, $\text{Lift}/q_\infty S_{ref}$

$C_{L,o}$ lift coefficient at $C_{D,min}$

C_{L_α} change of lift with angle of attack, $\partial C_L/\partial\alpha$, per degree

C_{l_β} change of rolling-moment coefficient with angle of sideslip, $\frac{C_{l_{\beta=3°}} - C_{l_{\beta=0°}}}{3}$, per degree

C_m pitching-moment coefficient, $\text{Pitching moment}/q_\infty S_{ref} L$

C_{n_β} change of yawing-moment coefficient with angle of sideslip, $\frac{C_{n_{\beta=3°}} - C_{n_{\beta=0°}}}{3}$, per degree

C_p coefficient of pressure, $\frac{p - p_\infty}{q_\infty}$

h altitude

K drag due to lift, $\partial C_D/\partial(C_L - C_{L,o})^2$

L body length, 0.701 m (27.6 in.)

L/D	lift-drag ratio, C_L/C_D
M	free-stream Mach number
N_{Re}	Reynolds number per unit length
p	static pressure
p_o	free-stream total pressure
p_∞	free-stream static pressure
q_∞	free-stream dynamic pressure
R	radius
S	area
S_{ref}	reference area, approximately equal to area of orbiter theoretical main delta wing (0.0929 m^2 (1 ft^2))
T_o	free-stream total temperature
x	coordinate direction along body axis
x_{ac}	aerodynamic center location measured from fuselage nose
α	angle of attack, deg
β	angle of sideslip, deg

DESCRIPTION OF MODEL

A photograph of the Spacejet model in the Langley Unitary Plan Wind Tunnel is shown in figure 2. A model drawing is shown in figure 3. The orbiter fuselage is of circular cross section with an area distribution based on the area-ruled full-scale concept previously described. The 55° leading-edge sweep, 8-percent-thick delta wing of the orbiter can accept the booster in a variety of positions as shown in figure 3. Model wing leading edges have a radius of 0.102 cm (0.040 in.). The gothic strake shown in figure 3 was designed by John E. Lamar using the procedure of reference 7 to maximize vortex lift at low speeds.

Twin orbiter vertical fins are located outboard of a possible opened shuttle-type payload door. Twin canted booster fins were designed to provide longitudinal as well as directional stability and control for booster-alone flight. Only limited tests were conducted with the fins in place, primarily to determine any adverse effects on drag and lift.

Booster pods are of circular cross section with constant-area, circular, flow-through ducts, as seen in figures 3 and 4. Notice in figure 4 that the cross-sectional area at the booster-pod exit is larger than the area of the duct, resulting in a booster base area. This base area was pressure instrumented to facilitate base drag corrections to the data.

A numerical model of the Spacejet wind-tunnel model is presented in table I. This listing is in the format described in reference 8 (Wave Drag Input).

EXPERIMENTAL PROCEDURE

Tests were conducted in the Langley Unitary Plan Wind Tunnel at Mach numbers of 1.50, 2.00, and 2.86. In order to obtain a minimum drag profile across the Mach number range, a few configurations were also tested at Mach numbers of 1.60, 1.70, and 2.36. The tests were conducted under the following conditions:

M	p_o		T_o		N_{Re}	
	kPa	psf	K	°R	per meter	per foot
1.50	53.5	1117	339	610	6.56×10^6	2.00×10^6
1.60	54.8	1144	↓	↓	↓	↓
1.70	56.4	1179				
2.00	63.5	1326				
2.36	75.5	1577				
2.86	98.4	2055				

Boundary-layer transition inducing strips of No. 50 sand grit were applied 1.016 cm (0.40 in.) streamwise behind the leading edge of all wings, fins, strakes, boosters, and booster ducts. A strip was also applied to the orbiter body 3.048 cm (1.20 in.) aft of the nose. The grit size and location were selected according to the method of reference 9 to insure fully turbulent boundary-layer flow aft of the transition inducing strips. Skin-friction drag on the booster ducts was estimated by the method of reference 10 and was removed from all measured axial forces. Forces and moments on the model were measured by means of a six-component strain-gage balance contained within the model. The balance was connected through a supporting sting to the permanent model actuating system in the wind tunnel. The angle-of-attack range was from -4° to 15° at 0° and 3° sideslip. The angle of attack was corrected for tunnel airflow misalignment and for deflection of the sting and balance under load.

Pressures were measured on the bases of both the orbiter and the boosters, and the experimental data were corrected to free-stream static pressure on these bases. A representative set of these measurements is shown in figure 5. (Note that this figure includes data from tests on this same model made in the Langley 8-Foot Transonic Pressure Tunnel.) The two sketches in the top right of the figure show cross-sectional views of the base of the orbiter and a booster; the sketches also show the location of the pressure measurements and,

in the case of the orbiter, the cross-sectional area of the two different stings used. In calculating the orbiter base drag, the pressures measured at the location of tubes 1 and 2 were assumed to act over areas 1 and 2, respectively, while the balance chamber pressure was assumed to act over the body cavity area. For the booster base, the pressure was measured by a circular manifold with four holes in it, as shown in figure 5. This pressure was assumed to act over the whole base area, exclusive of the opened duct. The pressure coefficients at each location are plotted in the figure as a function of Mach number. For reference, the parameter $-1/M^2$, which corresponds to a 0.7 vacuum pressure coefficient, is also plotted.

DISCUSSION

Drag Characteristics

The drag on a vehicle can be divided into two components: a minimum drag and a drag component due to lift. In the case of the Spacejet, the most important of these is the minimum drag because the flight trajectory involves a low angle-of-attack supersonic acceleration in order to maximize thrust minus drag. Supersonic zero-lift wave drag for the model was calculated by the far-field wave drag theory of reference 11 which analyzes the overall system area distribution and is not concerned with the details of local surface interaction. This method of wave drag analysis determines the average wave drag for a series of equivalent bodies which are formed by calculating the cross-sectional area distributions of the complete configuration along Mach planes. A computer-generated drawing of the geometry input to this program is shown in figure 6. All parts of the configuration are represented except for the booster strakes, which contribute only negligibly to total cross-sectional area and, because of program limitations, are not included.

The theoretical results have shown surprisingly good agreement with experiment especially when considering the complexity of the model. Figure 7 presents a comparison of experimental data and theoretical results for the model without fins for the boosters in four different positions. The theoretical drag consists of a wave drag contribution calculated by the method of reference 11 and a skin-friction contribution calculated by the T-prime method (ref. 10). Notice the reduction in drag as the boosters are moved forward, especially at the lower Mach numbers. According to the supersonic area rule theory, lowering the maximum cross-sectional area and/or smoothing the area distribution curve results in a lower wave drag. Such an effect can be seen in figure 8, which is an example of area-distribution contours calculated by the program of reference 11 for the numerical model without fins at a Mach number of 1.50. Notice that as the boosters move aft, the longitudinal changes in cross-sectional area become more severe, which implies increasing drag. Inspection of the curves in figure 7 shows this to be true. The forward booster position produces the lowest drag and is seen here to have the smoothest area distribution. The theoretical wave drag for any booster location at a particular Mach number could perhaps be reduced by employing an optimum area distribution for that Mach number; however, this could cause an undesirable drag increase at other Mach numbers and could reduce the overall efficiency of the total acceleration trajectory. In general, it can be seen that the drag of

this vehicle is sensitive to area-ruling effects. Furthermore, these effects can be predicted especially well at the lower Mach numbers where thrust-minus-drag levels become very critical.

Theoretical and experimental minimum drag variation with Mach number for the configuration buildup is shown in figure 9. Orbiter-alone drag is well predicted by theory. Addition of the boosters causes some mismatch between theory and experiment, with further discrepancy accompanying the addition of fins.

In general, however, the agreement between theory and experiment was good considering the complexity of the model and the many possibilities for local flow-separation effects. Schlieren photographs (fig. 10) show no obvious regions of undesirable subsonic flow. In particular, the booster inlets are seen to be started, and the booster exit flows appear supersonic.

Oil-flow tests of the model with fins and with boosters at the inboard nominal position were conducted at Mach numbers of 1.50 and 2.86 with a fluorescent-oil technique. Photographs of typical oil-flow patterns are shown in figure 11. Overall, no large areas of flow separation appear. Top views of the model reveal an interaction between orbiter vertical fins and disturbances emanating from the orbiter strake-wing intersection. Considerable flow angularity about the fins is also evident from the asymmetrical flow patterns produced by the orbiter fins on adjacent wing surfaces. These local flow interactions are, of course, not treated in the far-field wave drag theory of reference 11 and, for that reason, are likely to contribute to the overall discrepancy between theory and experiment noted in the discussion of figure 9. Views of the model lower surface at $M = 1.50$ (fig. 11(a)) show a small separated region on the orbiter body center line near the intersection of booster-pod shock waves. This separation region apparently disappears at the higher Mach numbers.

Lift Characteristics

Comparisons between the theoretical lifting surface method of reference 12 and angle-of-attack data at supersonic speeds are shown in figure 12. The upper diagram in figure 12 illustrates the input planforms of the orbiter-booster combination and the orbiter alone. The orbiter boosters were represented as an uncambered flat plate with a planform equivalent to the subtended outline of the orbiter boosters. The orbiter alone was input similarly. Considering the simplicity of the representation, agreement between theory and experiment is surprisingly good - implying that in those regions where the boosters overlap the orbiter, mutual cancellation of forces occurs. It should be pointed out that experimental-data values correspond to a model angle of attack of 4°, the likely attitude of the vehicle during acceleration. At higher angles of attack, the experimental pitching moment is not well predicted by lifting-surface theory as used in this paper.

Comparison of Linear Theory and Impact Theory

Figure 13 presents the theoretical results from linear theory and impact theory and the experimental data at Mach numbers of 2.00 and 2.86. The impact methods were applied through a modified version of the program of references 13 and 14. A discussion of these modifications can be found in the appendix of reference 15. The compressive impact methods consisted of tangent-cone theory over the orbiter and booster bodies and tangent-wedge theory applied to the wing and strake surfaces. Prandtl-Meyer expansion pressures were used on all lee-side surfaces. Skin friction for the impact methods was calculated within the program by the method of Spalding and Chi (ref. 16). In general, lift and drag forces were better predicted by using linear theory techniques than by using impact theory methods. These impact methods do not consider mutual interference effects such as between the orbiter and booster surfaces; however, interference is accounted for in the wave drag program of reference 11 and was implicitly assumed in the lifting-surface program of reference 12 by representing the geometry as a single planar surface. Pitching moments are better predicted by impact theory although neither theory could be considered accurate, especially at the higher angles of attack and lower Mach number ($M = 2.00$). It is understandable that as the Mach number increases, flow interactions between boosters and orbiter decrease as a result of the more highly swept nature of Mach angles and shock waves. The impact methods, which do not account for these mutual flow interactions, become more accurate at the higher Mach numbers.

Lateral-Directional Characteristics

Figure 14 presents experimental results for lateral and directional stability parameters. It is interesting to note that the destabilizing effect on lateral stability C_{l_β} of adding the booster to the orbiter is almost negated by the addition of the orbiter and booster fins.

Directional stability C_{n_β} of the orbiter is not changed appreciably by the addition of the boosters. This is because the booster is conceptually designed to be longitudinally located in the vicinity of the orbiter's center of gravity. The addition of fins to the orbiter and boosters do provide large margins of positive directional stability throughout the supersonic speed range.

Effect of Orbiter Wing Vertical Position

As mentioned previously (also see ref. 6), the Spacejet concept was area-ruled by reducing the orbiter body cross-sectional area distribution in the vicinity of the orbiter wing and boosters. The standard, or low-wing version of the orbiter is the one shown in figures 2 and 3. For this version the reduced fuselage area is separated from the boosters by the orbiter wing planform. The far-field wave drag program of reference 11 treats all geometrical components as transparent; thus, for example, the orbiter body above the wing can theoretically interact aerodynamically with the boosters below this wing.

To test these assumptions of wave drag theory and to investigate other interactions between a close-coupled orbiter body and booster, a high-wing arrangement of the Spacejet model without fins was tested. Figure 15 presents a comparison of the minimum drag of the high-wing and low-wing configurations. As can be seen, the difference in the drag levels is negligible. Indirectly, the similarity of the two results implies that separated flow problems caused by local interactions are of a minor nature on this configuration.

Experimental Longitudinal Aerodynamic Characteristics

The aerodynamic characteristics of all model configurations tested are presented in figures 16 to 29. Each figure presents the data for one configuration at Mach numbers of 1.50, 2.00, and 2.86. Included in each figure are six plots: lift coefficient, drag coefficient, and moment coefficient as functions of angle of attack and drag coefficient, moment coefficient, and lift-drag ratio as functions of lift coefficient. The figures are presented in the following order (for a description of model nomenclature, see the appendix):

CONCLUDING REMARKS

Predictions from standard linear supersonic drag theories were in very good agreement with experimental data for a complex vehicle having multiple bodies and wing surfaces in close proximity to one another. These results, in conjunction with flow-visualization studies, indicate that separated flow problems caused by local interactions are of a minor nature on this configuration.

The application of area-ruling principles for selecting booster location was found to have a very significant effect on supersonic drag levels. Small changes in booster fore and aft location had very significant effects on drag.

Impact theory was not as effective as linear theory in predicting the aerodynamic characteristics of the vehicle.

Langley Research Center
National Aeronautics and Space Administration
Hampton, VA 23665
June 9, 1981

APPENDIX

MODEL NOMENCLATURE

The model nomenclature used to describe the various configurations of the Spacejet is outlined below. (Also, see fig. 3.)

Orbiter or booster:

O	orbiter
B	booster

Component:

B	body of orbiter
P	pod of booster
W	wing
S	strake
F	fins

Orbiter wing position:

LW	low wing
HW	high wing

Booster position:

IN	inboard nominal
IF	inboard forward
IA	inboard aft
ON	outboard nominal

For example:

O(B+W+S)LW + B(P+W+S)IN

↓ ↓

Orbiter with body + wing + strake, low wing

Booster with pod + wing + strake, positioned at inboard nominal location on orbiter wing

REFERENCES

1. Henry, Beverly Z.; and Decker, John P.: Future Earth Orbit Transportation Systems/Technology Implications. Astronaut. & Aeronaut., vol. 14, no. 9, Sept. 1976, pp. 18-28.

2. A Collection of Technical Papers - AIAA/NASA Conference on Advanced Technology for Future Space Systems. May 1979.

3. Jackson, L. Robert; Martin, James A.; and Small, William J.: A Fully Reusable, Horizontal Takeoff Space Transport Concept With Two Small Turbojet Boosters. NASA TM-74087, 1977.

4. Martin, James A.: Use of a Duct-Burning Turbofan for an Earth-to-Orbit Vehicle Booster. AIAA Paper No. 79-1405, May 1979.

5. Hepler, A. K.; Zeck, H.; Walker, W.; and Scharf, W.: A Turbojet-Boosted Two-Stage-to-Orbit Space Transportation System Design Study. NASA CR-159018, 1979.

6. Small, W. J.; Riebe, G. D.; and Taylor, A. H.: Aerodynamics of a Turbojet-Boosted Launch Vehicle Concept. J. Spacecr. & Rockets, vol. 18, no. 1, Jan.-Feb. 1981, pp. 36-43.

7. Lamar, John E.: Analysis and Design of Strake-Wing Configurations. J. Aircr., vol. 17, no. 1, Jan. 1980, pp. 20-27.

8. Craidon, Charlotte B.: Description of a Digital Computer Program for Airplane Configuration Plots. NASA TM X-2074, 1970.

9. Braslow, Albert L.; Hicks, Raymond M.; and Harris, Roy V., Jr.: Use of Grit-Type Boundary-Layer-Transition Trips on Wind-Tunnel Models. NASA TN D-3579, 1966.

10. Sommer, Simon C.; and Short, Barbara J.: Free-Flight Measurements of Turbulent-Boundary-Layer Skin Friction in the Presence of Severe Aerodynamic Heating at Mach Numbers From 2.8 to 7.0. NACA TN 3391, 1955.

11. Harris, Roy V., Jr.: An Analysis and Correlation of Aircraft Wave Drag. NASA TM X-947, 1964.

12. Middleton, Wilbur D.; and Carlson, Harry W.: A Numerical Method for Calculating the Flat-Plate Pressure Distributions on Supersonic Wings of Arbitrary Planform. NASA TN D-2570, 1965.

13. Gentry, Arvel E.: Hypersonic Arbitrary-Body Aerodynamic Computer Program (Mark III Version). Vol. I - User's Manual. Rep. DAC 61552, Vol. I (Air Force Contract Nos. F33615 67 C 1008 and F33615 67 C 1602), McDonnell Douglas Corp., Apr. 1968. (Available from DTIC as AD 851 811.)

14. Gentry, Arvel E.; and Smyth, Douglas N.: Hypersonic Arbitrary-Body Aerodynamic Computer Program (Mark III Version). Vol. II - Program Formulation and Listings. Rep. DAC 61552, Vol. II (Air Force Contract Nos. F33615 67 C 1008 and F33615 67 C 1602), McDonnell Douglas Corp., Apr. 1968. (Available from DTIC as AD 851 812.)

15. Pittman, Jimmy L. (appendix by C. L. W. Edwards): Application of Supersonic Linear Theory and Hypersonic Impact Methods to Three Nonslender Hypersonic Airplane Concepts at Mach Numbers From 1.10 to 2.86. NASA TP-1539, 1979.

16. Spalding, D. B.; and Chi, S. W.: The Drag of a Compressible Turbulent Boundary Layer on a Smooth Flat Plate With and Without Heat Transfer. J. Fluid Mech., vol. 18, pt. 1, Jan. 1964, pp. 117-143.

TABLE I.- NUMERICAL DESCRIPTION OF SPACEJET MODEL

[See reference 8]

(a) Dimensions in centimeters

```
SPACEJET MODEL    INBOARD NOMINAL    WITH STRAKES
  1  1  1  1  1  0 16 23  1 13 20  0  0  0  0  0  0  1 11  4 10  2 10
365.76
  0.000    .039    .144    .302    .492  6.029 11.560 17.085 22.600 28.116  XAF   23
33.629 39.145 44.666 50.189 55.718 61.250 66.788 72.328 77.867 83.404  XAF   23
88.937 94.468100.000                                                     XAF   23
 12.06    2.59   -1.75   61.14                                           WAFORG 5
 18.42    4.87   -1.75   54.77                                           WAFORG 6
 25.30    6.08   -1.75   47.89                                           WAFORG 7
 34.15    7.30   -1.75   39.04                                           WAFORG 8
 47.19    8.51   -1.75   26.00                                           WAFORG 9
 48.92    9.73   -1.75   24.26                                           WAFORG10
 50.66   10.95   -1.75   22.52                                           WAFORG11
 52.40   12.16   -1.75   20.78                                           WAFORG12
 54.14   13.38   -1.75   19.04                                           WAFORG13
 55.87   14.60   -1.75   17.30                                           WAFORG14
 57.61   15.81   -1.75   15.56                                           WAFORG15
 59.35   17.03   -1.75   13.82                                           WAFORG16
 61.08   18.24   -1.75   12.08                                           WAFORG17
 62.82   19.46   -1.75   10.35                                           WAFORG18
 64.56   20.68   -1.75    8.61                                           WAFORG19
 66.30   21.89   -1.75    6.87                                           WAFORG20
  0.00   -0.01   -0.01   -0.01  -0.01  -0.02  -0.04  -0.05  -0.05  -0.04  TZORD  5
 -0.03   -0.01   -0.00    0.01   0.01   0.02   0.02   0.02   0.02   0.02  TZORD  5
  0.01    0.01    0.00                                                    TZORD  5
  0.00    0.00    0.00    0.00   0.00   0.00   0.00   0.00   0.00   0.00  TZORD  6
  0.00    0.00    0.00    0.00   0.00   0.00   0.00   0.00   0.00   0.00  TZORD  6
  0.00    0.00    0.00                                                    TZORD  6
  0.00    0.00    0.00    0.00   0.00   0.00   0.00   0.00   0.00   0.00  TZORD  7
  0.00    0.00    0.00    0.00   0.00   0.00   0.00   0.00   0.00   0.00  TZORD  7
  0.00    0.00    0.00                                                    TZORD  7
  0.00    0.00    0.00    0.00   0.00   0.00   0.00   0.00   0.00   0.00  TZORD  8
  0.00    0.00    0.00    0.00   0.00   0.00   0.00   0.00   0.00   0.00  TZORD  8
  0.00    0.00    0.00                                                    TZORD  8
  0.00    0.00    0.00    0.00   0.00   0.00   0.00   0.00   0.00   0.00  TZORD  9
  0.00    0.00    0.00    0.00   0.00   0.00   0.00   0.00   0.00   0.00  TZORD  9
  0.00    0.00    0.00                                                    TZORD  9
  0.00    0.00    0.00    0.00   0.00   0.00   0.00   0.00   0.00   0.00  TZORD 10
  0.00    0.00    0.00    0.00   0.00   0.00   0.00   0.00   0.00   0.00  TZORD 10
  0.00    0.00    0.00                                                    TZORD 10
  0.00    0.00    0.00    0.00   0.00   0.00   0.00   0.00   0.00   0.00  TZORD 11
  0.00    0.00    0.00    0.00   0.00   0.00   0.00   0.00   0.00   0.00  TZORD 11
  0.00    0.00    0.00                                                    TZORD 11
  0.00    0.00    0.00    0.00   0.00   0.00   0.00   0.00   0.00   0.00  TZORD 12
  0.00    0.00    0.00    0.00   0.00   0.00   0.00   0.00   0.00   0.00  TZORD 12
  0.00    0.00    0.00                                                    TZORD 12
  0.00    0.00    0.00    0.00   0.00   0.00   0.00   0.00   0.00   0.00  TZORD 13
  0.00    0.00    0.00    0.00   0.00   0.00   0.00   0.00   0.00   0.00  TZORD 13
```

TABLE I.- Continued

(a) Continued

0.00	0.00	0.00								TZORD 13
0.00	0.00	0.00	0.00	0.00	0.00	0.00	0.00	0.00	0.00	TZORD 14
0.00	0.00	0.00	0.00	0.00	0.00	0.00	0.00	0.00	0.00	TZORD 14
0.00	0.00	0.00								TZORD 14
0.00	0.00	0.00	0.00	0.00	0.00	0.00	0.00	0.00	0.00	TZORD 15
0.00	0.00	0.00	0.00	0.00	0.00	0.00	0.00	0.00	0.00	TZORD 15
0.00	0.00	0.00								TZORD 15
0.00	0.00	0.00	0.00	0.00	0.00	0.00	0.00	0.00	0.00	TZORD 16
0.00	0.00	0.00	0.00	0.00	0.00	0.00	0.00	0.00	0.00	TZORD 16
0.00	0.00	0.00								TZORD 16
0.00	0.00	0.00	0.00	0.00	0.00	0.00	0.00	0.00	0.00	TZORD 17
0.00	0.00	0.00	0.00	0.00	0.00	0.00	0.00	0.00	0.00	TZORD 17
0.00	0.00	0.00								TZORD 17
0.00	0.00	0.00	0.00	0.00	0.00	0.00	0.00	0.00	0.00	TZORD 18
0.00	0.00	0.00	0.00	0.00	0.00	0.00	0.00	0.00	0.00	TZORD 18
0.00	0.00	0.00								TZORD 18
0.00	0.00	0.00	0.00	0.00	0.00	0.00	0.00	0.00	0.00	TZORD 19
0.00	0.00	0.00	0.00	0.00	0.00	0.00	0.00	0.00	0.00	TZORD 19
0.00	0.00	0.00								TZORD 19
0.00	0.00	0.00	0.00	0.00	0.00	0.00	0.00	0.00	0.00	TZORD 20
0.00	0.00	0.00	0.00	0.00	0.00	0.00	0.00	0.00	0.00	TZORD 20
0.00	0.00	0.00								TZORD 20
0.000	.004	.015	.030	.046	.260	.260	.260	.260	.260	WAFORD 5
.260	.260	.328	1.120	1.537	2.036	2.237	2.239	2.089	1.791	WAFORD 5
1.335	.740	-.000								WAFORD 5
0.000	.004	.014	.030	.049	.290	.290	.290	.290	.290	WAFORD 6
.290	.290	.368	1.108	1.663	2.040	2.260	2.277	2.149	1.849	WAFORD 6
1.340	.742	-.000								WAFORD 6
0.000	.004	.014	.030	.049	.263	.332	.332	.332	.332	WAFORD 7
.332	.332	1.111	1.591	2.046	2.320	2.459	2.426	2.275	1.936	WAFORD 7
1.485	.793	-.000								WAFORD 7
0.000	.004	.014	.030	.049	.195	.407	.407	.407	.407	WAFORD 8
.778	1.555	2.082	2.394	2.716	2.822	2.839	2.678	2.494	1.952	WAFORD 8
1.549	.716	-.000								WAFORD 8
0.000	.160	.295	.376	.409	1.186	1.867	2.453	2.943	3.340	WAFORD 9
3.643	3.854	3.972	3.997	3.929	3.767	3.512	3.163	2.720	2.182	WAFORD 9
1.550	.823	-.000								WAFORD 9
0.000	.167	.308	.395	.433	1.206	1.884	2.466	2.953	3.347	WAFORD10
3.648	3.857	3.973	3.996	3.927	3.765	3.509	3.160	2.717	2.179	WAFORD10
1.548	.822	-.000								WAFORD10
0.000	.175	.322	.418	.461	1.230	1.903	2.481	2.965	3.356	WAFORD11
3.654	3.860	3.974	3.996	3.925	3.762	3.505	3.156	2.713	2.176	WAFORD11
1.545	.820	-.000								WAFORD11
0.000	.184	.339	.445	.494	1.257	1.925	2.499	2.979	3.366	WAFORD12
3.661	3.864	3.976	3.996	3.923	3.759	3.502	3.152	2.709	2.172	WAFORD12
1.542	.819	-.000								WAFORD12
0.000	.195	.361	.476	.533	1.290	1.952	2.520	2.995	3.378	WAFORD13
3.669	3.869	3.977	3.995	3.921	3.755	3.497	3.146	2.703	2.167	WAFORD13
1.539	.816	-.000								WAFORD13
0.000	.209	.385	.512	.577	1.329	1.984	2.546	3.015	3.392	WAFORD14
3.679	3.874	3.979	3.994	3.918	3.750	3.491	3.140	2.697	2.162	WAFORD14
1.534	.814	-.000								WAFORD14
0.000	.216	.401	.542	.623	1.376	2.022	2.576	3.038	3.409	WAFORD15
3.690	3.881	3.982	3.993	3.913	3.744	3.483	3.132	2.689	2.155	WAFORD15
1.529	.811	-.000								WAFORD15
0.000	.208	.418	.579	.681	1.435	2.070	2.614	3.067	3.430	WAFORD16
3.704	3.888	3.984	3.991	3.908	3.736	3.474	3.122	2.679	2.146	WAFORD16
1.522	.807	0.000								WAFORD16

TABLE I.- Continued

(a) Continued

0.000	.209	.445	.627	.756	1.511	2.132	2.663	3.104	3.457	WAFORD17	
3.721	3.898	3.987	3.988	3.901	3.725	3.461	3.108	2.666	2.134	WAFORD17	
1.513	.802	-.000								WAFORD17	
0.000	.218	.482	.694	.845	1.614	2.216	2.729	3.155	3.493	WAFORD18	
3.745	3.911	3.990	3.984	3.891	3.711	3.444	3.089	2.647	2.118	WAFORD18	
1.500	.795	-.000								WAFORD18	
0.000	.210	.529	.786	.936	1.760	2.334	2.823	3.225	3.543	WAFORD19	
3.777	3.928	3.994	3.976	3.875	3.688	3.418	3.062	2.620	2.094	WAFORD19	
1.482	.785	-.000								WAFORD19	
0.000	.212	.605	.865	1.076	1.983	2.514	2.964	3.331	3.618	WAFORD20	
3.824	3.950	3.996	3.962	3.847	3.651	3.375	3.016	2.577	2.055	WAFORD20	
1.452	.767	-.000								WAFORD20	
0.00	3.81	7.62	11.43	15.24	19.05	22.86	26.67	30.48	34.29	XFUS	20
38.10	41.91	45.72	49.53	53.34	57.15	60.96	64.77	68.58	70.10	XFUS	20
0.00	0.00	0.00	0.00	0.00	0.00	0.00	0.00	0.00	0.00	Y	1
0.00	0.00	0.00								Y	1
0.00	0.00	0.00	0.00	0.00	0.00	0.00	0.00	0.00	0.00	Z	1
0.00	0.00	0.00								Z	1
0.00	0.26	0.51	0.72	0.88	0.98	1.02	0.98	0.88	0.72	Y	2
0.51	0.26	0.00								Y	2
-1.02	-0.98	-0.88	-0.72	-0.51	-0.26	0.00	0.26	0.51	0.72	Z	2
0.88	0.98	1.02								Z	2
0.00	0.49	0.94	1.33	1.63	1.82	1.89	1.82	1.63	1.33	Y	3
0.94	0.49	0.00								Y	3
-1.89	-1.82	-1.64	-1.33	-0.94	-0.49	0.00	0.49	0.94	1.33	Z	3
1.64	1.82	1.89								Z	3
0.00	0.68	1.31	1.84	2.25	2.52	2.62	2.52	2.25	1.84	Y	4
1.31	0.68	0.00								Y	4
-2.62	-2.52	-2.27	-1.84	-1.30	-0.68	0.00	0.68	1.30	1.84	Z	4
2.27	2.52	2.62								Z	4
0.00	0.83	1.60	2.26	2.76	3.09	3.21	3.09	2.76	2.26	Y	5
1.60	0.83	0.00								Y	5
-3.21	-3.09	-2.78	-2.26	-1.60	-0.83	0.00	0.83	1.60	2.26	Z	5
2.78	3.09	3.21								Z	5
0.00	0.94	1.83	2.58	3.15	3.53	3.66	3.53	3.15	2.58	Y	6
1.83	0.94	0.00								Y	6
-3.66	-3.53	-3.17	-2.58	-1.82	-0.94	0.00	0.94	1.82	2.58	Z	6
3.17	3.53	3.66								Z	6
0.00	1.03	1.99	2.80	3.43	3.84	3.99	3.84	3.43	2.80	Y	7
1.99	1.03	0.00								Y	7
-3.99	-3.84	-3.45	-2.81	-1.98	-1.03	0.00	1.03	1.98	2.81	Z	7
3.45	3.84	3.99								Z	7
0.00	1.08	2.09	2.94	3.60	4.02	4.18	4.02	3.60	2.94	Y	8
2.09	1.08	0.00								Y	8
-4.18	-4.03	-3.62	-2.94	-2.08	-1.08	0.00	1.08	2.08	2.94	Z	8
3.62	4.03	4.18								Z	8
0.00	1.09	2.12	2.99	3.65	4.08	4.24	4.08	3.65	2.99	Y	9
2.12	1.09	0.00								Y	9
-4.24	-4.09	-3.67	-2.99	-2.11	-1.09	0.00	1.09	2.11	2.99	Z	9
3.67	4.09	4.24								Z	9
0.00	1.09	2.10	2.97	3.65	4.07	4.22	4.06	3.63	2.97	Y	10
2.11	1.09	0.00								Y	10
-4.22	-4.06	-3.63	-2.97	-2.11	-1.09	0.00	1.09	2.10	2.97	Z	10
3.65	4.07	4.22								Z	10
0.00	1.07	2.07	2.92	3.57	3.99	4.15	3.99	3.57	2.92	Y	11
2.07	1.07	0.00								Y	11
-4.15	-4.00	-3.59	-2.92	-2.06	-1.07	0.00	1.07	2.06	2.92	Z	11
3.59	4.00	4.15								Z	11

TABLE I.- Continued

(a) Concluded

```
  0.00   1.04   2.01   2.83   3.46   3.87   4.03   3.87   3.46   2.83  Y      12
  2.01   1.04   0.00                                                   Y      12
 -4.03  -3.88  -3.48  -2.84  -2.00  -1.04   0.00   1.04   2.00   2.84  Z      12
  3.48   3.88   4.03                                                   Z      12
  0.00   0.99   1.92   2.72   3.34   3.72   3.86   3.71   3.32   2.72  Y      13
  1.93   1.00   0.00                                                   Y      13
 -3.86  -3.71  -3.32  -2.72  -1.93  -1.00   0.00   0.99   1.92   2.72  Z      13
  3.34   3.72   3.86                                                   Z      13
  0.00   0.94   1.82   2.56   3.13   3.50   3.64   3.50   3.13   2.56  Y      14
  1.82   0.94   0.00                                                   Y      14
 -3.64  -3.51  -3.15  -2.56  -1.81  -0.94   0.00   0.94   1.81   2.56  Z      14
  3.15   3.51   3.64                                                   Z      14
  0.00   0.87   1.68   2.36   2.89   3.23   3.36   3.23   2.89   2.36  Y      15
  1.68   0.87   0.00                                                   Y      15
 -3.36  -3.24  -2.91  -2.36  -1.67  -0.87   0.00   0.87   1.67   2.36  Z      15
  2.91   3.24   3.36                                                   Z      15
  0.00   0.82   1.58   2.23   2.72   3.05   3.16   3.05   2.72   2.23  Y      16
  1.58   0.82   0.00                                                   Y      16
 -3.16  -3.05  -2.74  -2.23  -1.57  -0.82   0.00   0.82   1.57   2.23  Z      16
  2.74   3.05   3.16                                                   Z      16
  0.00   0.80   1.55   2.18   2.67   2.98   3.10   2.98   2.67   2.18  Y      17
  1.55   0.80   0.00                                                   Y      17
 -3.10  -2.99  -2.68  -2.18  -1.54  -0.80   0.00   0.80   1.54   2.18  Z      17
  2.68   2.99   3.10                                                   Z      17
  0.00   0.85   1.64   2.32   2.83   3.16   3.29   3.16   2.83   2.32  Y      18
  1.64   0.85   0.00                                                   Y      18
 -3.29  -3.17  -2.85  -2.32  -1.64  -0.85   0.00   0.85   1.64   2.32  Z      18
  2.85   3.17   3.29                                                   Z      18
  0.00   0.93   1.81   2.55   3.11   3.48   3.62   3.49   3.13   2.55  Y      19
  1.80   0.93   0.00                                                   Y      19
 -3.62  -3.49  -3.13  -2.55  -1.80  -0.93   0.00   0.93   1.81   2.55  Z      19
  3.11   3.48   3.62                                                   Z      19
  0.00   0.95   1.84   2.59   3.17   3.55   3.68   3.55   3.17   2.59  Y      20
  1.84   0.95   0.00                                                   Y      20
 -3.68  -3.55  -3.19  -2.60  -1.83  -0.95   0.00   0.95   1.83   2.60  Z      20
  3.19   3.55   3.68                                                   Z      20
 42.67  11.89  -7.62                                                   PODORG1
  0.00   1.52   3.05   6.10   9.14  10.67  12.19  13.72  15.24  18.29    XPOD1
 21.03                                                                  XPODI
  2.11   2.56   2.90   3.38   3.66   3.74   3.75   3.71   3.62   3.33    PODR1
  2.95                                                                  PODR1
 61.47   6.35  -1.27  15.11  79.45   6.35  11.28   6.20                 FINORG1
0.     6.7    17.074 27.439 37.807 53.352 68.9   79.266 89.631 100.0     XFIN1
0.     1.967  2.496  2.836  2.992  2.873  2.336  1.746  .967   0.0     FINORD1
 52.07  11.89  -4.15  11.05  57.78  11.89  -2.06  11.05                 FINORG2
0.0    11.11  22.222 33.333 44.444 55.56  66.66  77.777 88.900 100.     XFIN2
0.     2.40   4.160  5.340  5.93   5.93   5.340  4.160  2.400  0.      FINORD2
 65.13   9.78  -9.65   6.73  72.14   6.73  -4.32   2.54                 FINORG3
0.      .45   12.39  24.34  36.29  48.23  60.18  72.13  84.07  100.     XFIN3
0.      .577  1.848  2.748  3.06   3.464  2.864  2.714  1.801  0.      FINORD3
 65.13  14.00  -9.65   6.55  72.14  17.05  -4.32   2.54                 FINORG4
0.      .45   12.39  24.34  36.29  48.23  60.18  72.13  84.07  100.     XFIN4
0.      .577  1.848  2.748  3.06   3.464  2.864  2.714  1.801  0.      FINORD4
 61.88   0.63  -8.64   4.11  50.66   8.46  -8.64  15.34                 CANORG1
0.      .2654 12.24  24.21  36.18  48.14  60.11  72.08  84.04  100.     XCAN1
0.      .309  1.475  2.309  2.815  3.     2.852  2.383  1.58   0.      CANORD1
 50.66  15.32  -8.64  15.34  61.88  23.14  -8.64   4.11                 CANORG2
0.      .2654 12.24  24.21  36.18  48.14  60.11  72.08  84.04  100.     XCAN2
0.      .309  1.475  2.309  2.815  3.     2.852  2.383  1.58   0.      CANORD2
```

TABLE I.- Continued

(b) Dimensions in inches

```
SPACEJET MODEL   INBOARD NOMINAL   WITH STRAKES
  1  1  1  1  1  0 16 23  1 13 20  0  0  0  0  0  0  1 11  4 10  2 10
144.00
 0.000   .039   .144   .302   .492  6.029 11.560 17.085 22.600 28.116  XAF   23
33.629 39.145 44.666 50.189 55.718 61.250 66.788 72.328 77.867 83.404  XAF   23
88.937 94.468100.000                                                  XAF   23
 4.748  1.021  -.690 24.069                                           WAFORG 5
 7.251  1.916  -.690 21.564                                           WAFORG 6
 9.960  2.394  -.690 18.855                                           WAFORG 7
13.444  2.873  -.690 15.370                                           WAFORG 8
18.579  3.352  -.690 10.235                                           WAFORG 9
19.261  3.831  -.690  9.550                                           WAFORG10
19.945  4.310  -.690  8.866                                           WAFORG11
20.629  4.789  -.690  8.181                                           WAFORG12
21.313  5.268  -.690  7.496                                           WAFORG13
21.997  5.747  -.690  6.811                                           WAFORG14
22.681  6.226  -.690  6.127                                           WAFORG15
23.365  6.704  -.690  5.442                                           WAFORG16
24.049  7.183  -.690  4.757                                           WAFORG17
24.733  7.662  -.690  4.073                                           WAFORG18
25.417  8.141  -.690  3.388                                           WAFORG19
26.101  8.620  -.690  2.703                                           WAFORG20
 0.000  -.002  -.004  -.002  -.002  -.009  -.015  -.019  -.019  -.015  TZORD  5
 -.010  -.005  -.001   .003   .005   .008   .008   .008   .007   .006  TZORD  5
  .003   .002   .000                                                  TZORD  5
 0.000   .000   .000   .000   .000   .000   .000   .000   .000   .000  TZORD  6
 -.000  -.000  -.000   .000   .000  -.000  -.000   .000  -.000   .000  TZORD  6
  .000   .000   .000                                                  TZORD  6
 0.000   .000   .000   .000   .000   .000   .000  -.000  -.000  -.000  TZORD  7
  .000  -.000  -.000  -.000   .000  -.000   .000   .000  -.000   .000  TZORD  7
  .000   .000 0.000                                                  TZORD  7
 0.000   .000   .000   .000   .000   .000   .000  -.000  -.000  -.000  TZORD  8
 -.000  -.000  -.000   .000  -.000  -.000   .000  -.000   .000   .000  TZORD  8
  .000   .000   .000                                                  TZORD  8
 0.000   .000   .000   .000   .000   .000   .000   .000   .000   .000  TZORD  9
 -.000  -.000   .000  -.000  -.000   .000  -.000  -.000   .000   .000  TZORD  9
  .000   .000   .000                                                  TZORD  9
 0.000   .000   .000   .000   .000   .000   .000   .000   .000   .000  TZORD 10
  .000  -.000  -.000   .000  -.000   .000   .000   .000   .000   .000  TZORD 10
  .000   .000   .000                                                  TZORD 10
 0.000   .000   .000   .000   .000   .000   .000   .000   .000  -.000  TZORD 11
 -.000   .000   .000  -.000  -.000   .000   .000   .000   .000   .000  TZORD 11
  .000   .000   .000                                                  TZORD 11
 0.000   .000   .000   .000   .000   .000   .000   .000   .000   .000  TZORD 12
 -.000  -.000   .000  -.000  -.000  -.000   .000   .000   .000   .000  TZORD 12
  .000   .000 0.000                                                  TZORD 12
 0.000   .000   .000   .000   .000   .000   .000   .000   .000   .000  TZORD 13
  .000   .000   .000   .000   .000   .000   .000   .000   .000   .000  TZORD 13
```

TABLE I.- Continued

(b) Continued

.000	.000	.000								TZORD 13
0.000	.000	.000	.000	.000	.000	.000	.000	.000	.000	TZORD 14
.000	.000	.000	.000	.000	.000	.000	.000	.000	.000	TZORD 14
.000	.000	.000								TZORD 14
0.000	.000	.000	.000	.000	.000	.000	.000	.000	.000	TZORD 15
.000	.000	.000	.000	.000	.000	.000	.000	.000	.000	TZORD 15
.000	.000	.000								TZORD 15
0.000	.000	.000	.000	.000	.000	.000	.000	.000	.000	TZORD 16
.000	.000	.000	.000	.000	.000	.000	.000	.000	.000	TZORD 16
.000	.000	0.000								TZORD 16
0.000	.000	.000	.000	.000	.000	.000	.000	.000	.000	TZORD 17
.000	.000	.000	.000	.000	.000	.000	.000	.000	.000	TZORD 17
.000	.000	.000								TZORD 17
0.000	.000	.000	.000	.000	.000	.000	.000	.000	.000	TZORD 18
.000	.000	.000	.000	.000	.000	.000	.000	.000	.000	TZORD 18
.000	.000	.000								TZORD 18
0.000	.000	.000	.000	.000	.000	.000	.000	.000	.000	TZORD 19
.000	.000	.000	.000	.000	.000	.000	.000	.000	.000	TZORD 19
.000	.000	.000								TZORD 19
0.000	.000	.000	.000	.000	.000	.000	.000	.000	.000	TZORD 20
.000	.000	.000	.000	.000	.000	.000	.000	.000	.000	TZORD 20
.000	.000	.000								TZORD 20
0.000	.004	.015	.030	.046	.260	.260	.260	.260	.260	WAFORD 5
.260	.260	.328	1.120	1.537	2.036	2.237	2.239	2.089	1.791	WAFORD 5
1.335	.740	-.000								WAFORD 5
0.000	.004	.014	.030	.049	.290	.290	.290	.290	.290	WAFORD 6
.290	.290	.368	1.108	1.663	2.040	2.260	2.277	2.149	1.849	WAFORD 6
1.340	.742	-.000								WAFORD 6
0.000	.004	.014	.030	.049	.263	.332	.332	.332	.332	WAFORD 7
.332	.332	1.111	1.591	2.046	2.320	2.459	2.426	2.275	1.936	WAFORD 7
1.485	.793	-.000								WAFORD 7
0.000	.004	.014	.030	.049	.195	.407	.407	.407	.407	WAFORD 8
.778	1.555	2.082	2.394	2.716	2.822	2.839	2.678	2.494	1.952	WAFORD 8
1.549	.716	-.000								WAFORD 8
0.000	.160	.295	.376	.409	1.186	1.867	2.453	2.943	3.340	WAFORD 9
3.643	3.854	3.972	3.997	3.929	3.767	3.512	3.163	2.720	2.182	WAFORD 9
1.550	.823	-.000								WAFORD 9
0.000	.167	.308	.395	.433	1.206	1.884	2.466	2.953	3.347	WAFORD10
3.648	3.857	3.973	3.996	3.927	3.765	3.509	3.160	2.717	2.179	WAFORD10
1.548	.822	-.000								WAFORD10
0.000	.175	.322	.418	.461	1.230	1.903	2.481	2.965	3.356	WAFORD11
3.654	3.860	3.974	3.996	3.925	3.762	3.505	3.156	2.713	2.176	WAFORD11
1.545	.820	-.000								WAFORD11
0.000	.184	.339	.445	.494	1.257	1.925	2.499	2.979	3.366	WAFORD12
3.661	3.864	3.976	3.996	3.923	3.759	3.502	3.152	2.709	2.172	WAFORD12
1.542	.819	-.000								WAFORD12
0.000	.195	.361	.476	.533	1.290	1.952	2.520	2.995	3.378	WAFORD13
3.669	3.869	3.977	3.995	3.921	3.755	3.497	3.146	2.703	2.167	WAFORD13
1.539	.816	-.000								WAFORD13
0.000	.209	.385	.512	.577	1.329	1.984	2.546	3.015	3.392	WAFORD14
3.679	3.874	3.979	3.994	3.918	3.750	3.491	3.140	2.697	2.162	WAFORD14
1.534	.814	-.000								WAFORD14
0.000	.216	.401	.542	.623	1.376	2.022	2.576	3.038	3.409	WAFORD15
3.690	3.881	3.982	3.993	3.913	3.744	3.483	3.132	2.689	2.155	WAFORD15
1.529	.811	-.000								WAFORD15
0.000	.208	.418	.579	.681	1.435	2.070	2.614	3.067	3.430	WAFORD16
3.704	3.888	3.984	3.991	3.908	3.736	3.474	3.122	2.679	2.146	WAFORD16
1.522	.807	0.000								WAFORD16

TABLE I.- Continued

(b) Continued

0.000	.209	.445	.627	.756	1.511	2.132	2.663	3.104	3.457	WAFORD17	
3.721	3.898	3.987	3.988	3.901	3.725	3.461	3.108	2.666	2.134	WAFORD17	
1.513	.802	-.000								WAFORD17	
0.000	.218	.482	.694	.845	1.614	2.216	2.729	3.155	3.493	WAFORD18	
3.745	3.911	3.990	3.984	3.891	3.711	3.444	3.089	2.647	2.118	WAFORD18	
1.500	.795	-.000								WAFORD18	
0.000	.210	.529	.786	.936	1.760	2.334	2.823	3.225	3.543	WAFORD19	
3.777	3.928	3.994	3.976	3.875	3.688	3.418	3.062	2.620	2.094	WAFORD19	
1.482	.785	-.000								WAFORD19	
0.000	.212	.605	.865	1.076	1.983	2.514	2.964	3.331	3.618	WAFORD20	
3.824	3.950	3.996	3.962	3.847	3.651	3.375	3.016	2.577	2.055	WAFORD20	
1.452	.767	-.000								WAFORD20	
0.000	1.500	3.000	4.500	6.000	7.500	9.000	10.500	12.000	13.500	XFUS	20
15.000	16.500	18.000	19.500	21.000	22.500	24.000	25.500	27.000	27.600	XFUS	20
0.000	0.000	0.000	0.000	0.000	0.000	0.000	0.000	0.000	0.000	Y	1
0.000	0.000	0.000								Y	1
0.000	0.000	0.000	0.000	0.000	0.000	0.000	0.000	0.000	0.000	Z	1
0.000	0.000	0.000								Z	1
0.000	.104	.201	.283	.346	.386	.402	.386	.346	.283	Y	2
.201	.104	0.000								Y	2
-.402	-.387	-.348	-.283	-.200	-.104	0.000	.104	.200	.283	Z	2
.348	.387	.402								Z	2
0.000	.192	.372	.524	.641	.716	.744	.716	.641	.524	Y	3
.372	.192	0.000								Y	3
-.744	-.718	-.645	-.524	-.370	-.192	0.000	.192	.370	.524	Z	3
.645	.718	.744								Z	3
0.000	.266	.515	.726	.887	.992	1.031	.992	.887	.726	Y	4
.515	.266	0.000								Y	4
-1.031	-.994	-.893	-.726	-.513	-.266	0.000	.266	.513	.726	Z	4
.893	.994	1.031								Z	4
0.000	.326	.631	.889	1.087	1.215	1.263	1.215	1.087	.889	Y	5
.631	.326	0.000								Y	5
-1.263	-1.218	-1.094	-.890	-.628	-.326	0.000	.326	.628	.890	Z	5
1.094	1.218	1.263								Z	5
0.000	.372	.720	1.015	1.241	1.388	1.442	1.388	1.241	1.015	Y	6
.720	.372	0.000								Y	6
-1.442	-1.390	-1.249	-1.016	-.717	-.372	0.000	.372	.717	1.016	Z	6
1.249	1.390	1.442								Z	6
0.000	.405	.784	1.104	1.350	1.510	1.569	1.510	1.350	1.104	Y	7
.784	.405	0.000								Y	7
-1.569	-1.513	-1.359	-1.105	-.780	-.405	0.000	.405	.780	1.105	Z	7
1.359	1.513	1.569								Z	7
0.000	.424	.822	1.158	1.416	1.583	1.645	1.583	1.416	1.158	Y	8
.822	.424	0.000								Y	8
-1.645	-1.586	-1.425	-1.159	-.818	-.424	0.000	.424	.818	1.159	Z	8
1.425	1.586	1.645								Z	8
0.000	.431	.834	1.176	1.438	1.607	1.670	1.607	1.438	1.176	Y	9
.834	.431	0.000								Y	9
-1.670	-1.610	-1.446	-1.177	-.830	-.431	0.000	.431	.830	1.177	Z	9
1.446	1.610	1.670								Z	9
0.000	.428	.826	1.170	1.438	1.601	1.660	1.598	1.429	1.169	Y	10
.830	.429	0.000								Y	10
-1.660	-1.598	-1.429	-1.169	-.830	-.429	0.000	.428	.826	1.170	Z	10
1.438	1.601	1.660								Z	10
0.000	.421	.815	1.149	1.405	1.571	1.632	1.571	1.405	1.149	Y	11
.815	.421	0.000								Y	11
-1.632	-1.574	-1.414	-1.150	-.811	-.421	0.000	.421	.811	1.150	Z	11
1.414	1.574	1.632								Z	11

TABLE I.- Concluded

(b) Concluded

```
  0.000   .409   .792  1.115  1.364  1.525  1.585  1.525  1.364  1.115  Y      12
   .792   .409  0.000                                                  Y      12
-1.585 -1.528 -1.372 -1.117  -.788  -.409  0.000   .409   .788  1.117  Z      12
 1.372  1.528  1.585                                                  Z      12
  0.000   .391   .755  1.070  1.315  1.464  1.518  1.461  1.307  1.069  Y      13
   .758   .392  0.000                                                  Y      13
-1.518 -1.461 -1.307 -1.069  -.758  -.392  0.000   .391   .755  1.070  Z      13
 1.315  1.464  1.518                                                  Z      13
  0.000   .370   .716  1.009  1.233  1.379  1.433  1.379  1.233  1.009  Y      14
   .716   .370  0.000                                                  Y      14
-1.433 -1.382 -1.241 -1.009  -.712  -.369  0.000   .369   .712  1.009  Z      14
 1.241  1.382  1.433                                                  Z      14
  0.000   .341   .660   .930  1.137  1.272  1.321  1.272  1.137   .930  Y      15
   .660   .341  0.000                                                  Y      15
-1.321 -1.274 -1.144  -.931  -.657  -.341  0.000   .341   .657   .931  Z      15
 1.144  1.274  1.321                                                  Z      15
  0.000   .321   .622   .877  1.072  1.199  1.245  1.199  1.072   .877  Y      16
   .622   .321  0.000                                                  Y      16
-1.245 -1.201 -1.079  -.878  -.619  -.321  0.000   .321   .619   .878  Z      16
 1.079  1.201  1.245                                                  Z      16
  0.000   .315   .610   .859  1.050  1.174  1.220  1.174  1.050   .859  Y      17
   .610   .315  0.000                                                  Y      17
-1.220 -1.176 -1.057  -.860  -.607  -.315  0.000   .315   .607   .860  Z      17
 1.057  1.176  1.220                                                  Z      17
  0.000   .334   .647   .912  1.115  1.246  1.295  1.246  1.115   .912  Y      18
   .647   .334  0.000                                                  Y      18
-1.295 -1.249 -1.122  -.912  -.644  -.334  0.000   .334   .644   .912  Z      18
 1.122  1.249  1.295                                                  Z      18
  0.000   .368   .712  1.003  1.226  1.371  1.424  1.374  1.234  1.004  Y      19
   .708   .367  0.000                                                  Y      19
-1.424 -1.374 -1.234 -1.004  -.708  -.367  0.000   .368   .712  1.003  Z      19
 1.226  1.371  1.424                                                  Z      19
  0.000   .374   .724  1.021  1.248  1.396  1.450  1.396  1.248  1.021  Y      20
   .724   .374  0.000                                                  Y      20
-1.450 -1.398 -1.256 -1.022  -.721  -.374  0.000   .374   .721  1.022  Z      20
 1.256  1.398  1.450                                                  Z      20
16.8   4.68   -3.0                                                    PODORG1
0.0    .6     1.2    2.4    3.6    4.2    4.8    5.4    6.     7.2      XPOD1
8.28                                                                   XPOD1
.829   1.007  1.141  1.33   1.442  1.471  1.476  1.46   1.424  1.312    PODR1
1.16                                                                   PODR1
24.2   2.5    -.5    5.95   31.28  2.5    4.44   2.44                 FINORG1
0.     6.7    17.074 27.439 37.807 53.352 68.9   79.266 89.631 100.     XFIN1
0.     1.967  2.496  2.836  2.992  2.873  2.336  1.746  .967   0.0    FINORD1
20.5   4.68   -1.635 4.35   22.75  4.68   -.812  4.35                 FINORG2
0.0    11.11  22.222 33.333 44.444 55.56  66.66  77.777 88.900 100.     XFIN2
0.     2.40   4.160  5.340  5.93   5.93   5.340  4.160  2.400  0.     FINORD2
25.64  3.85   -3.8   2.65   28.4   2.65   -1.7   1.                   FINORG3
0.     .45    12.39  24.34  36.29  48.23  60.18  72.13  84.07  100.     XFIN3
0.     .577   1.848  2.748  3.06   3.464  2.864  2.714  1.801  0.     FINORD3
25.64  5.513  -3.8   2.58   28.4   6.713  -1.7   1.0                  FINORG4
0.     .45    12.39  24.34  36.29  48.23  60.18  72.13  84.07  100.     XFIN4
0.     .577   1.848  2.748  3.06   3.464  2.864  2.714  1.801  0.     FINORD4
24.363 .25    -3.4   1.62   19.943 3.33   -3.4   6.04                 CANORG1
0.     .2654  12.24  24.21  36.18  48.14  60.11  72.08  84.04  100.     XCAN1
0.     .309   1.475  2.309  2.815  3.     2.852  2.383  1.58   0.     CANORD1
19.943 6.03   -3.4   6.04   24.363  9.11  -3.4   1.62                 CANORG2
0.     .2654  12.24  24.21  36.18  48.14  60.11  72.08  84.04  100.     XCAN2
0.     .309   1.475  2.309  2.815  3.     2.852  2.383  1.58   0.     CANORD2
```

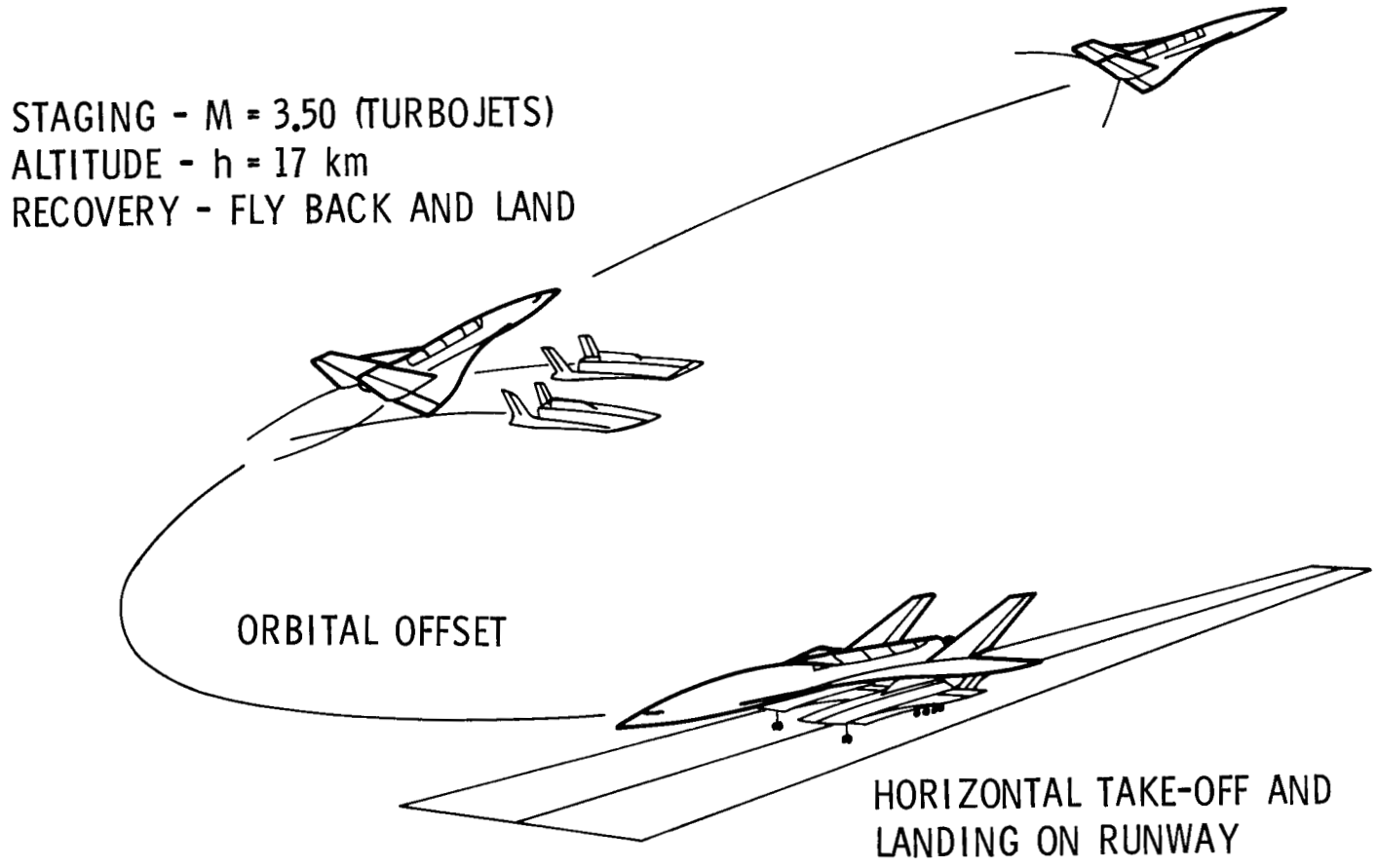

Figure 1.- Advanced space transportation concept (Spacejet).

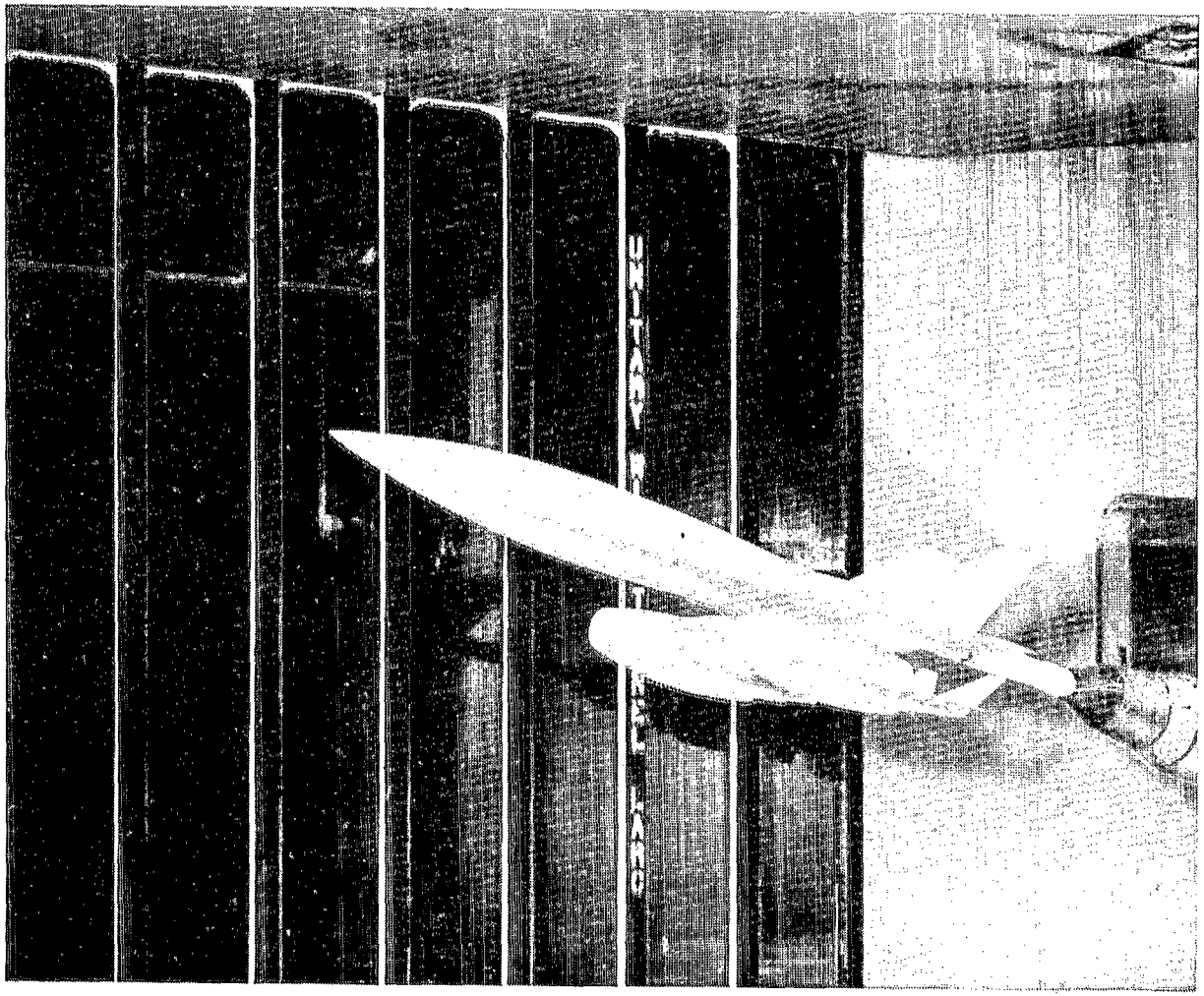

L-79-965

Figure 2.- Photograph of model in Langley Unitary Plan Wind Tunnel.

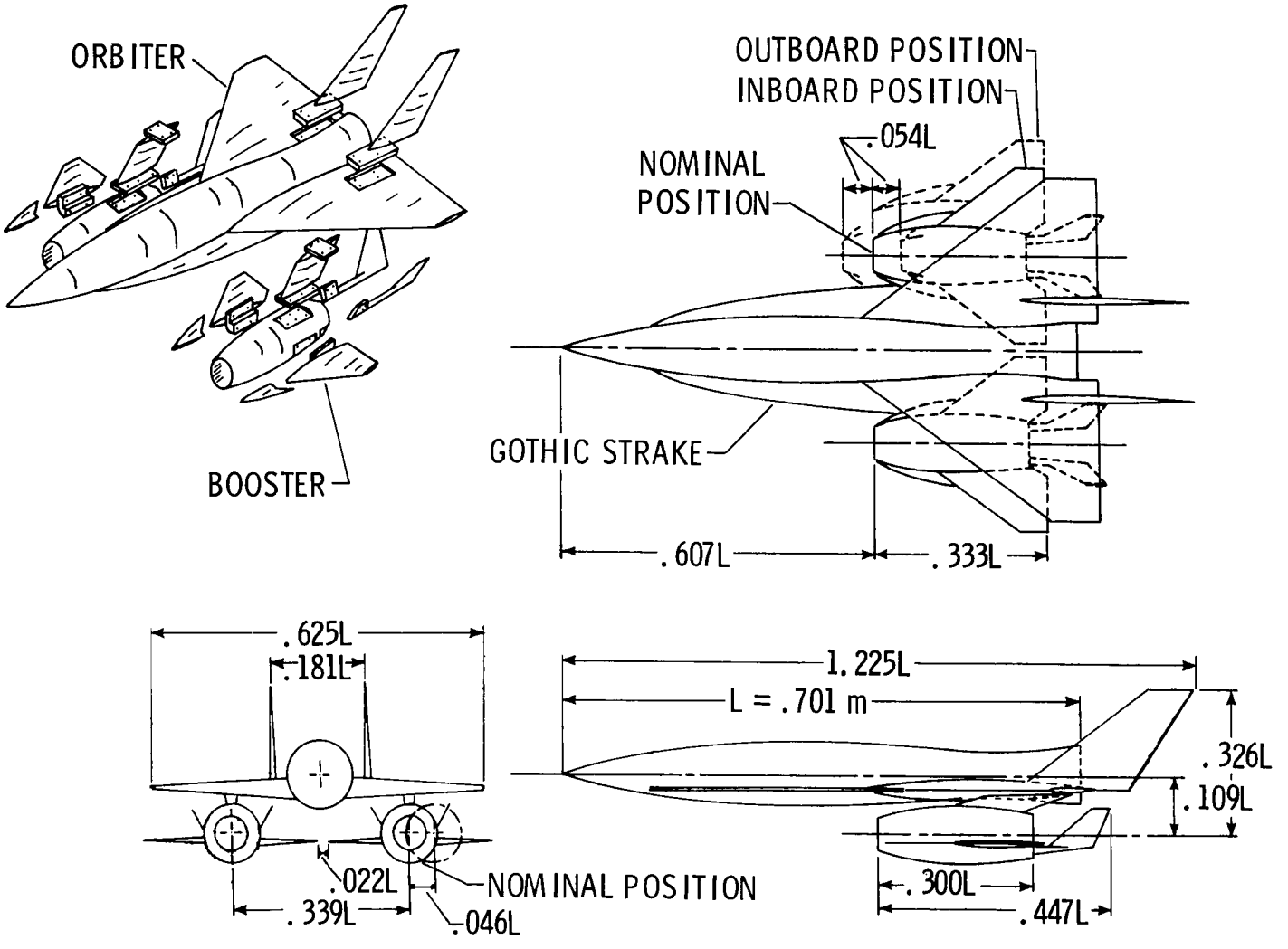

Figure 3.- Spacejet wind-tunnel model.

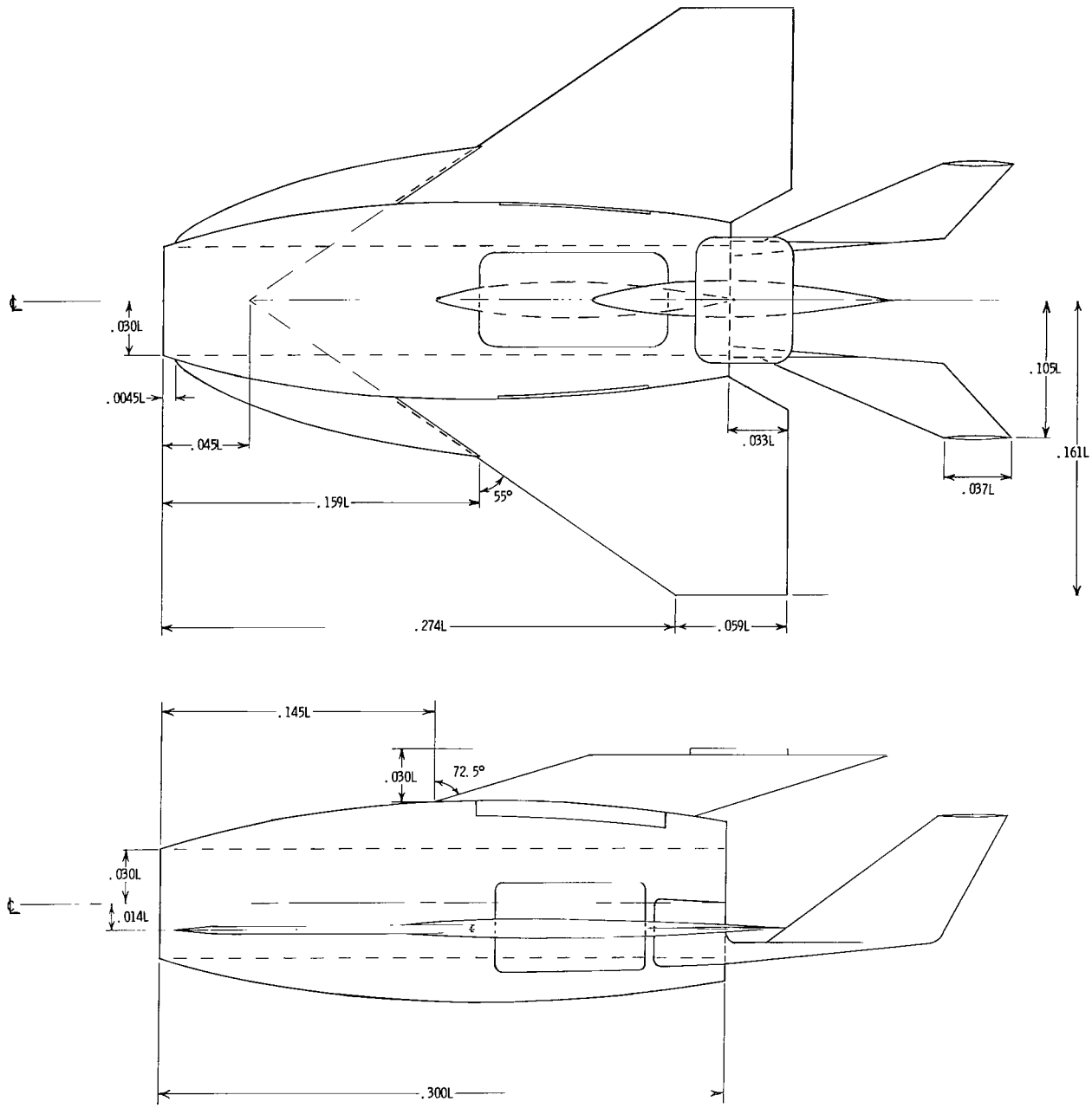

Figure 4.- Spacejet booster wind-tunnel model. L = 0.701 m.

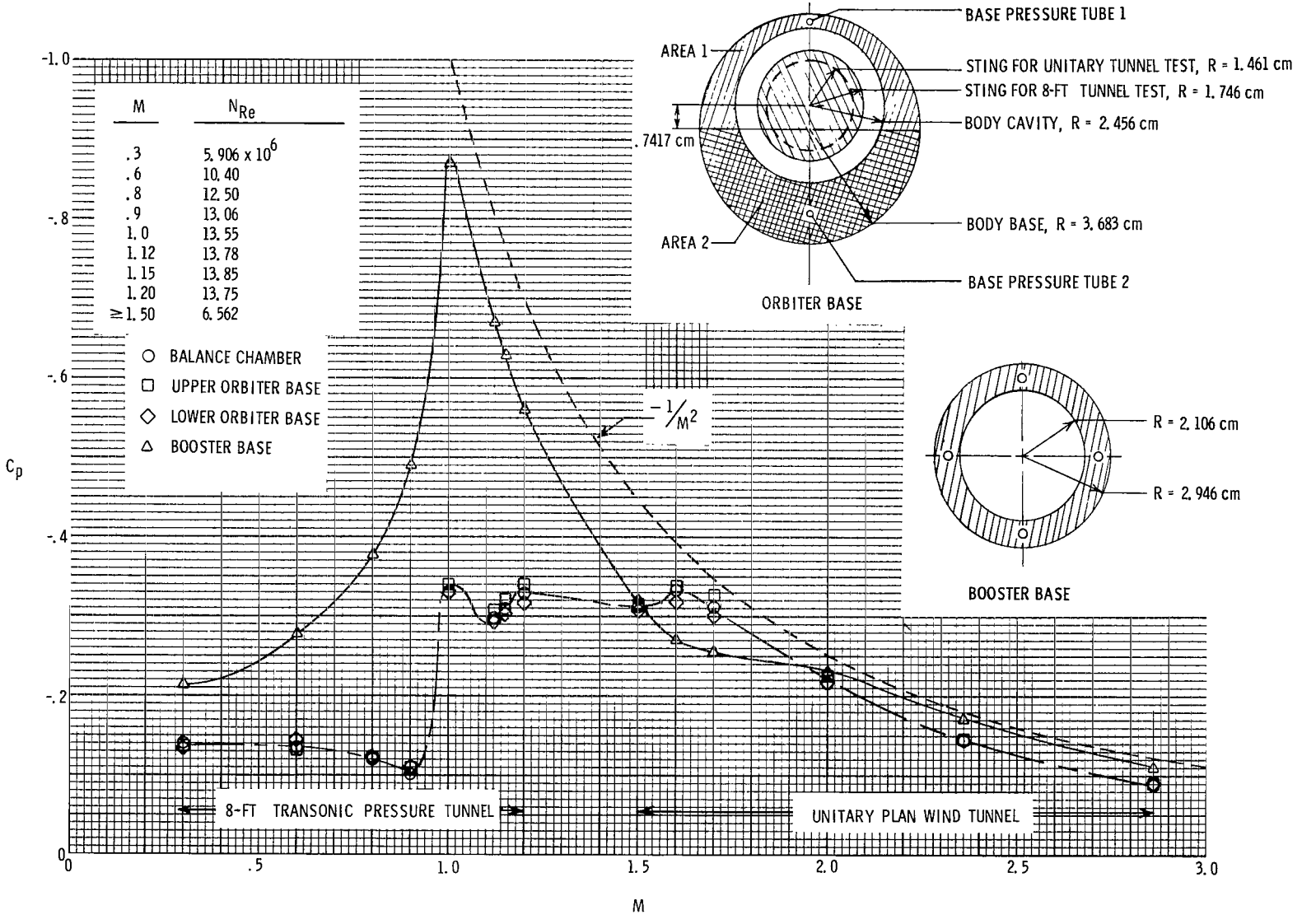

Figure 5.- Base and chamber pressure measurements. $\alpha = 0°$.

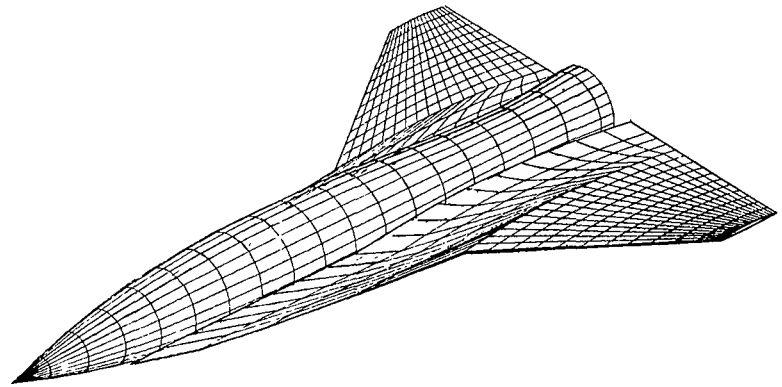

ORBITER BODY + WING + STRAKE

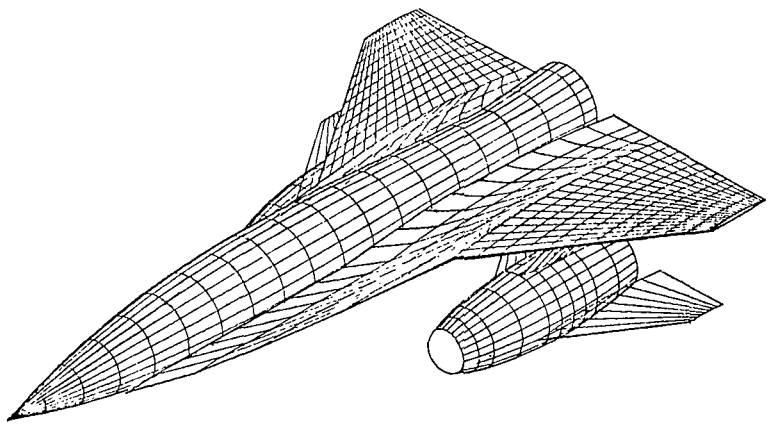

ORBITER + BOOSTERS

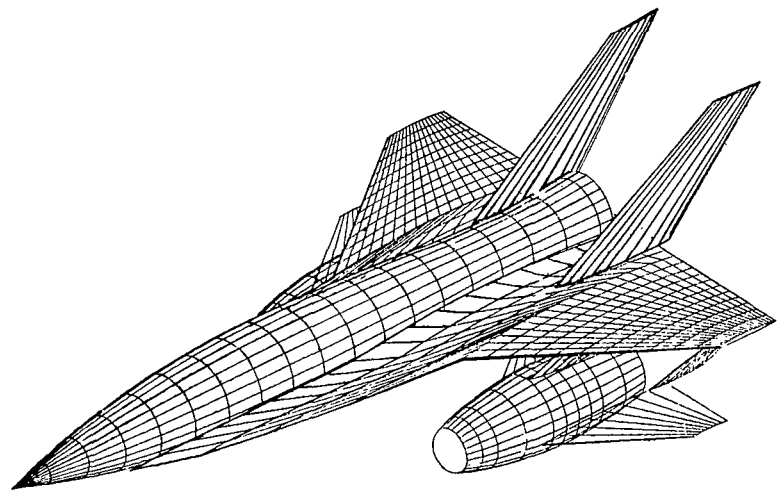

ORBITER + BOOSTERS + FINS

Figure 6.- Geometry representation of input to wave drag program of reference 11.

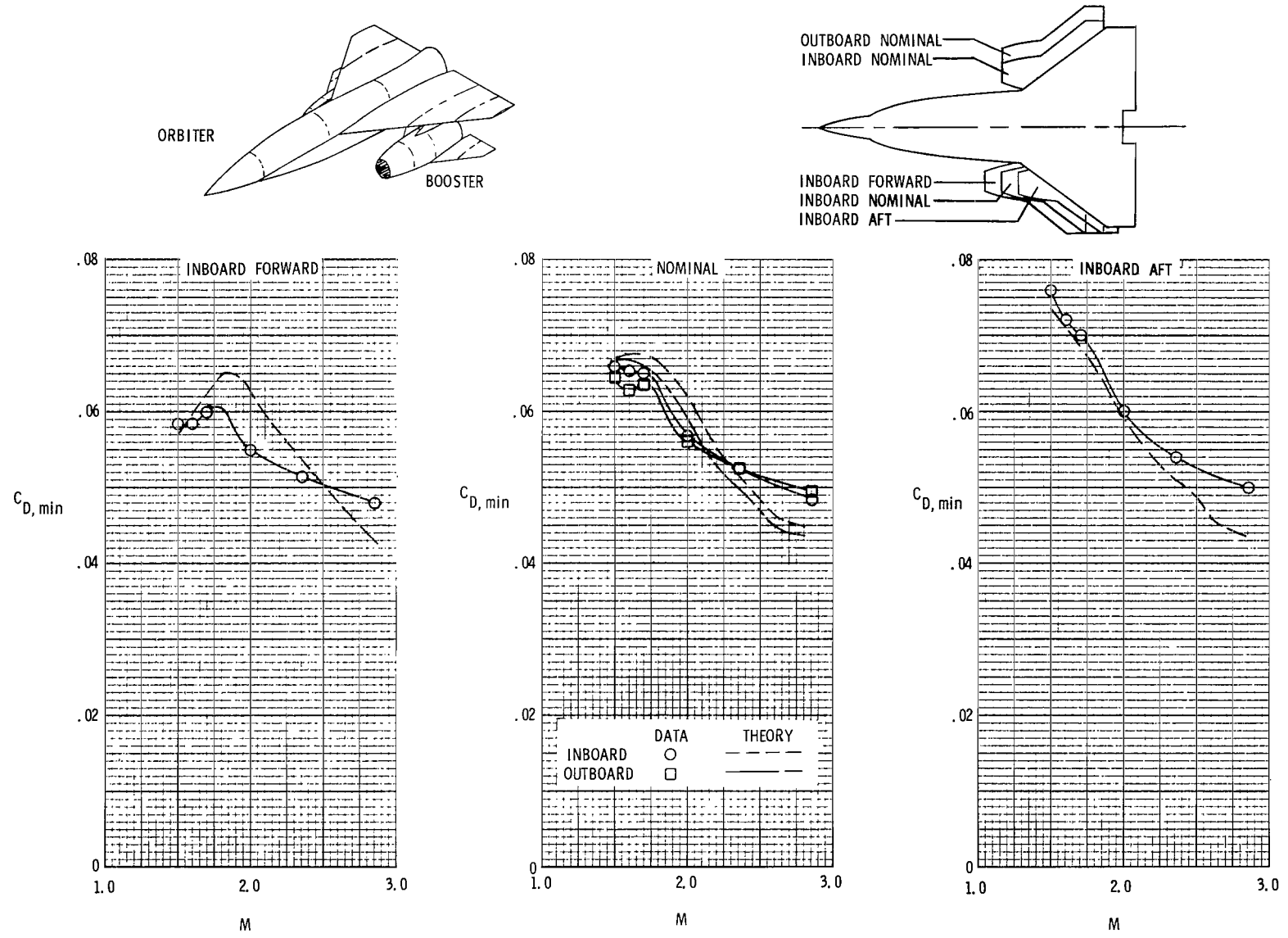

Figure 7.- Booster location effects on minimum drag.

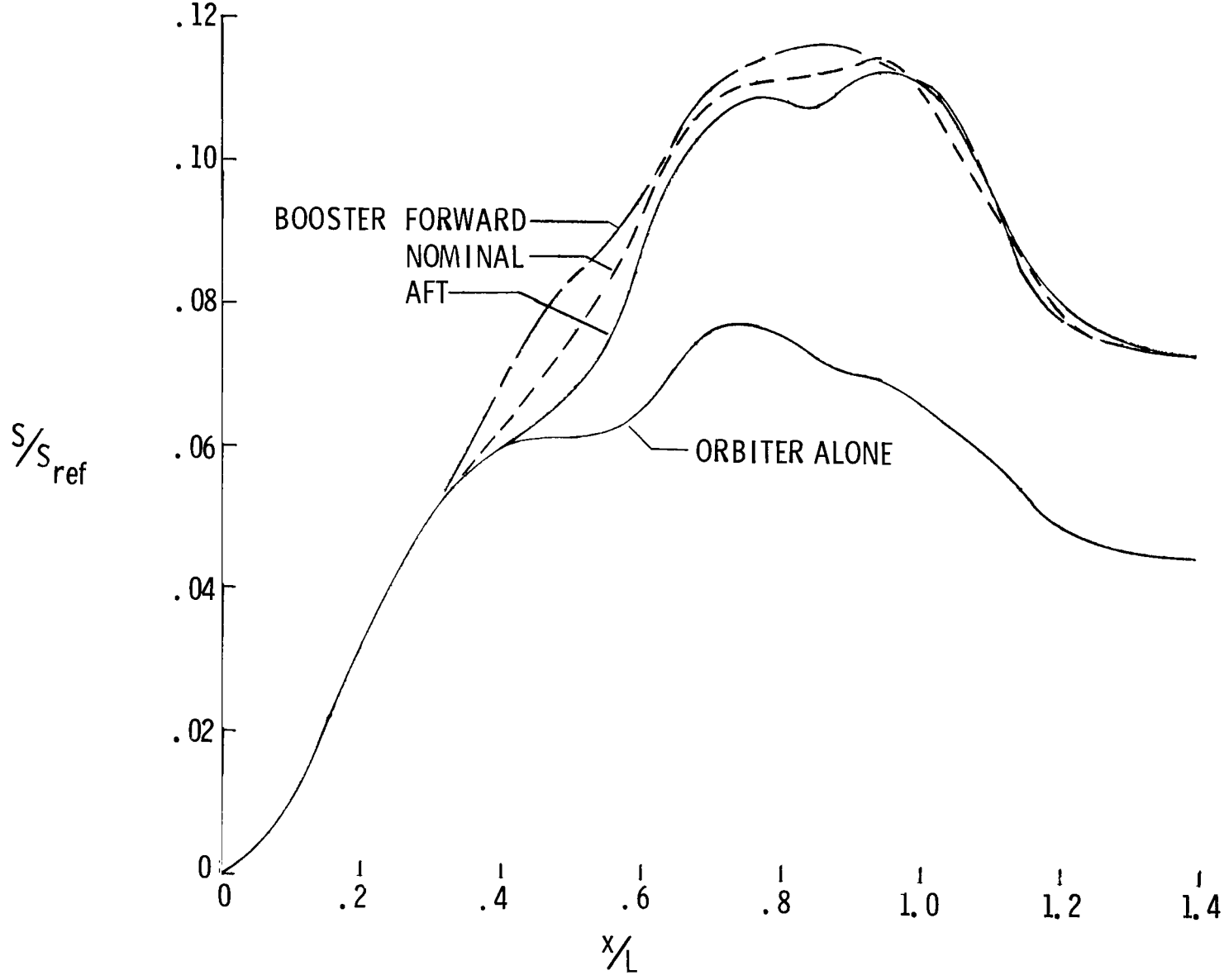

Figure 8.- Equivalent body area distribution for different inboard booster locations. M = 1.50; without fins.

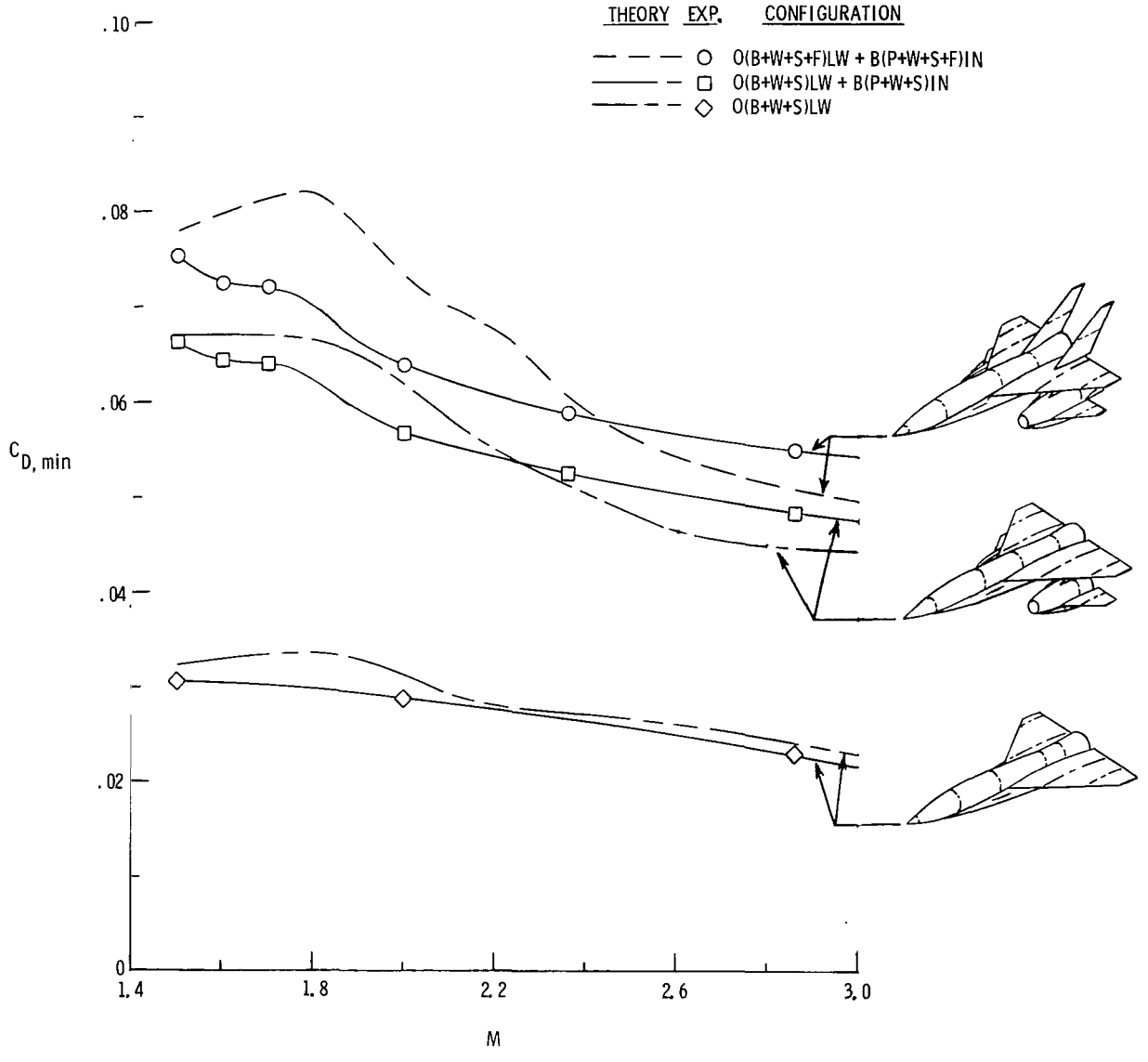

Figure 9.- Effect of configuration buildup on minimum drag.

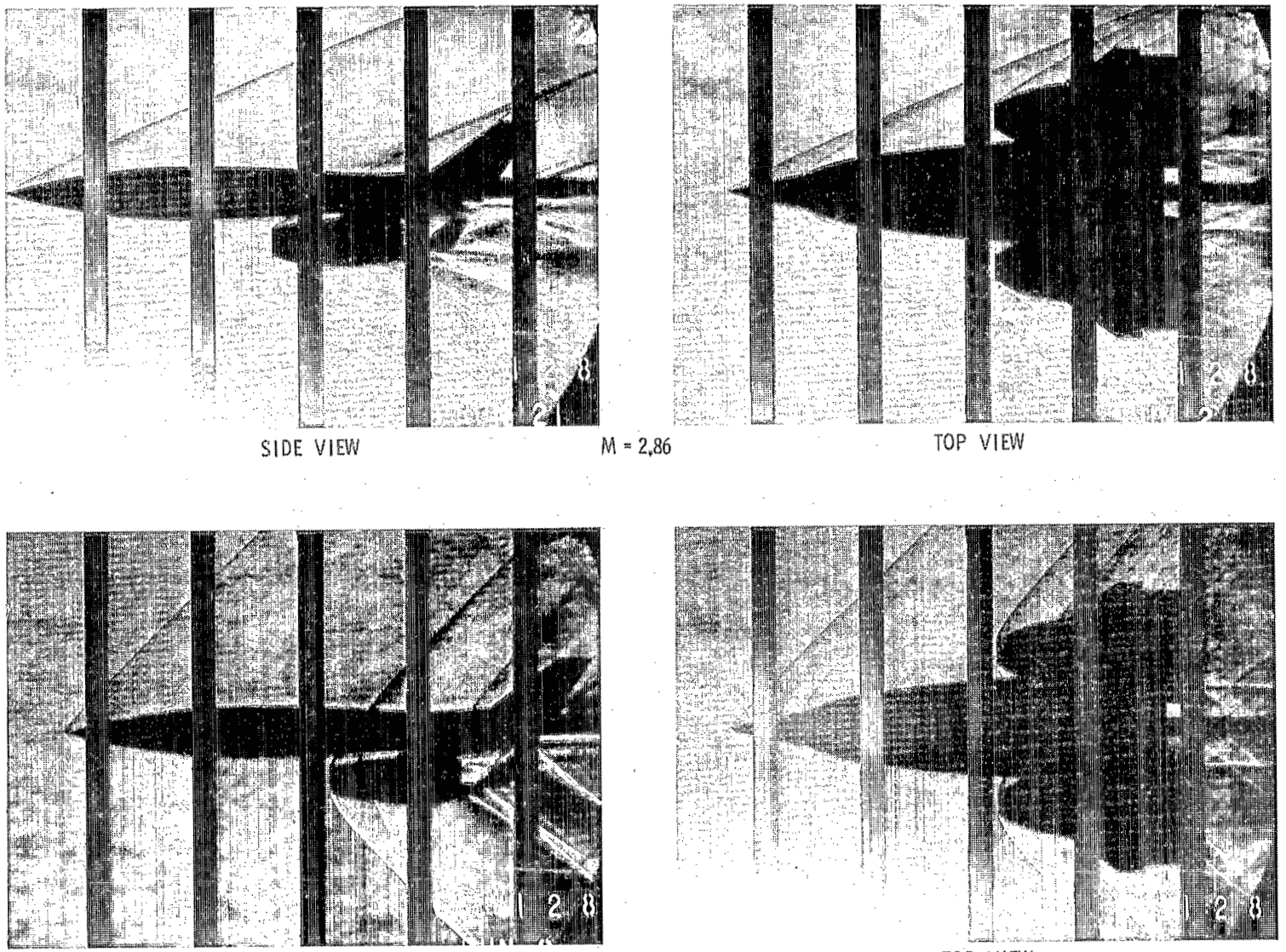

Figure 10.- Schlieren photographs of O(B+W+S+F)LW + B(P+W+S+F)IN configuration. $\alpha = 0°$.

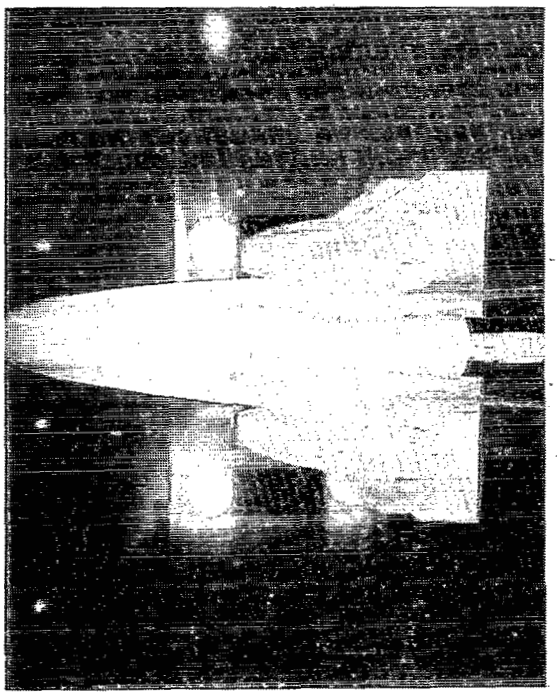

TOP VIEW
$\alpha = 0^0$

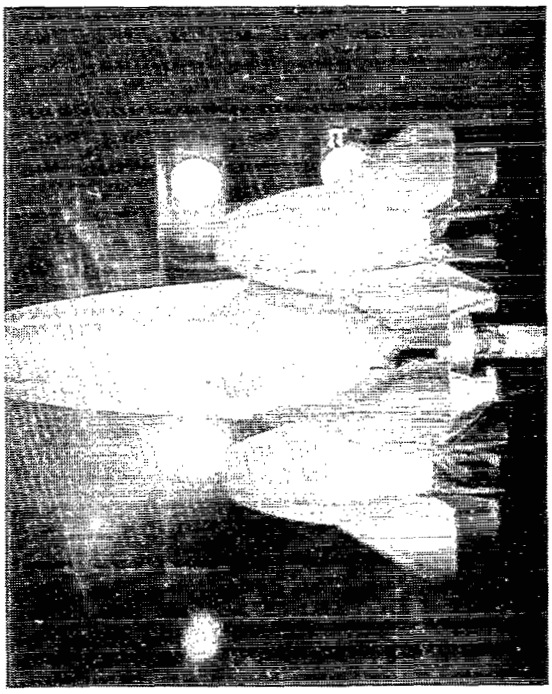

BOTTOM VIEW
$\alpha = 0^0$

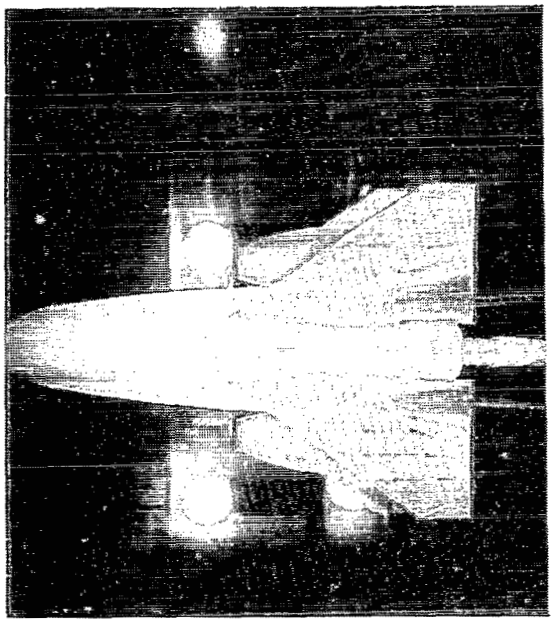

TOP VIEW
$\alpha = 4^0$

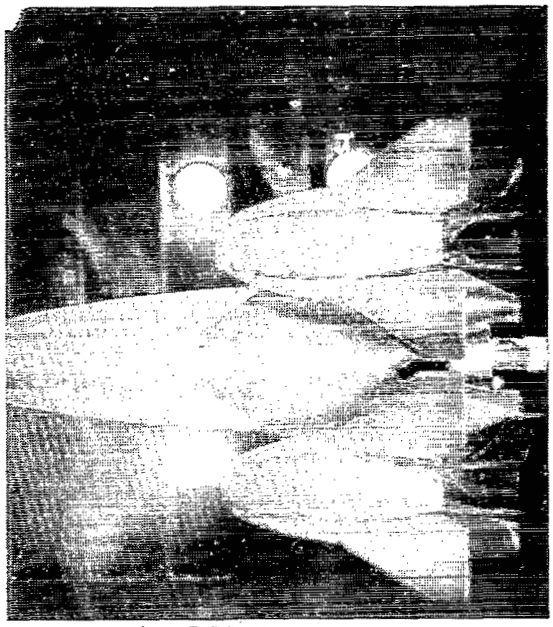

BOTTOM VIEW
$\alpha = 4^0$

L-81-162

(a) M = 1.50.

Figure 11.- Oil-flow patterns of O(B+W+S+F)LW + B(P+W+S+F)IN configuration.

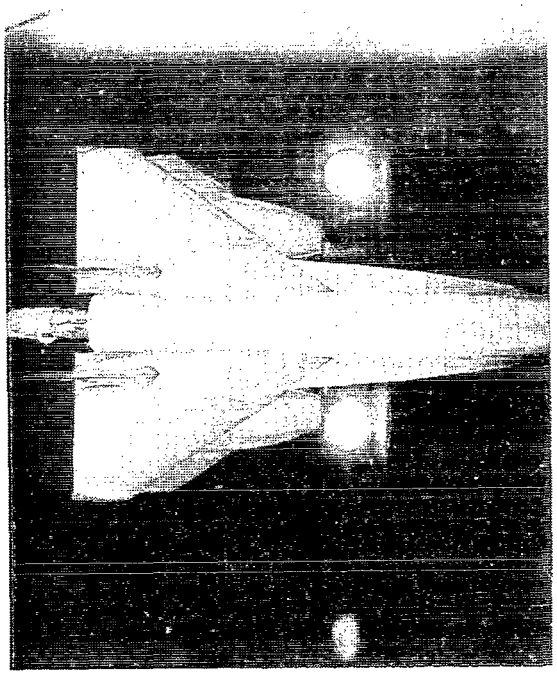

TOP VIEW
$\alpha = 0^0$

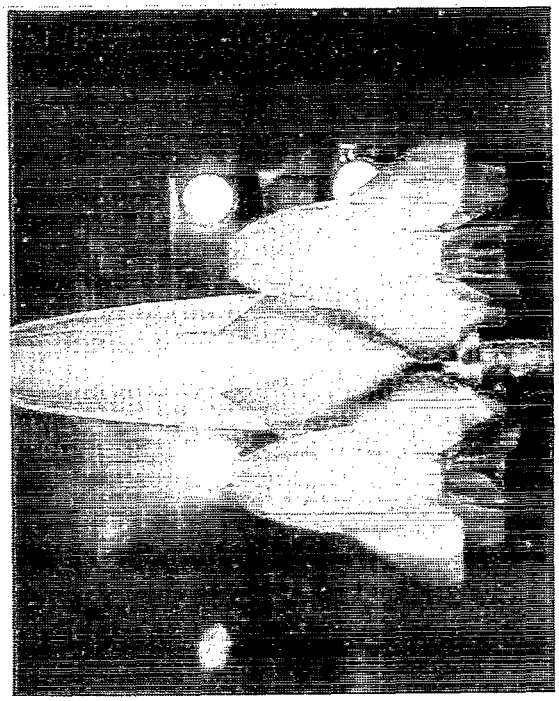

BOTTOM VIEW
$\alpha = 0^0$

SIDE VIEWS
$\alpha = 0^0$

L-81-163

(b) M = 2.86.

Figure 11.- Concluded.

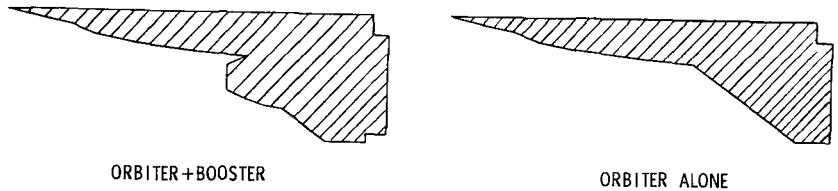

PLANFORMS INPUT TO PROGRAM OF REF. 12

THEORY	EXP.	CONFIGURATION
– – –	○	ORBITER+BOOSTERS
———	□	ORBITER

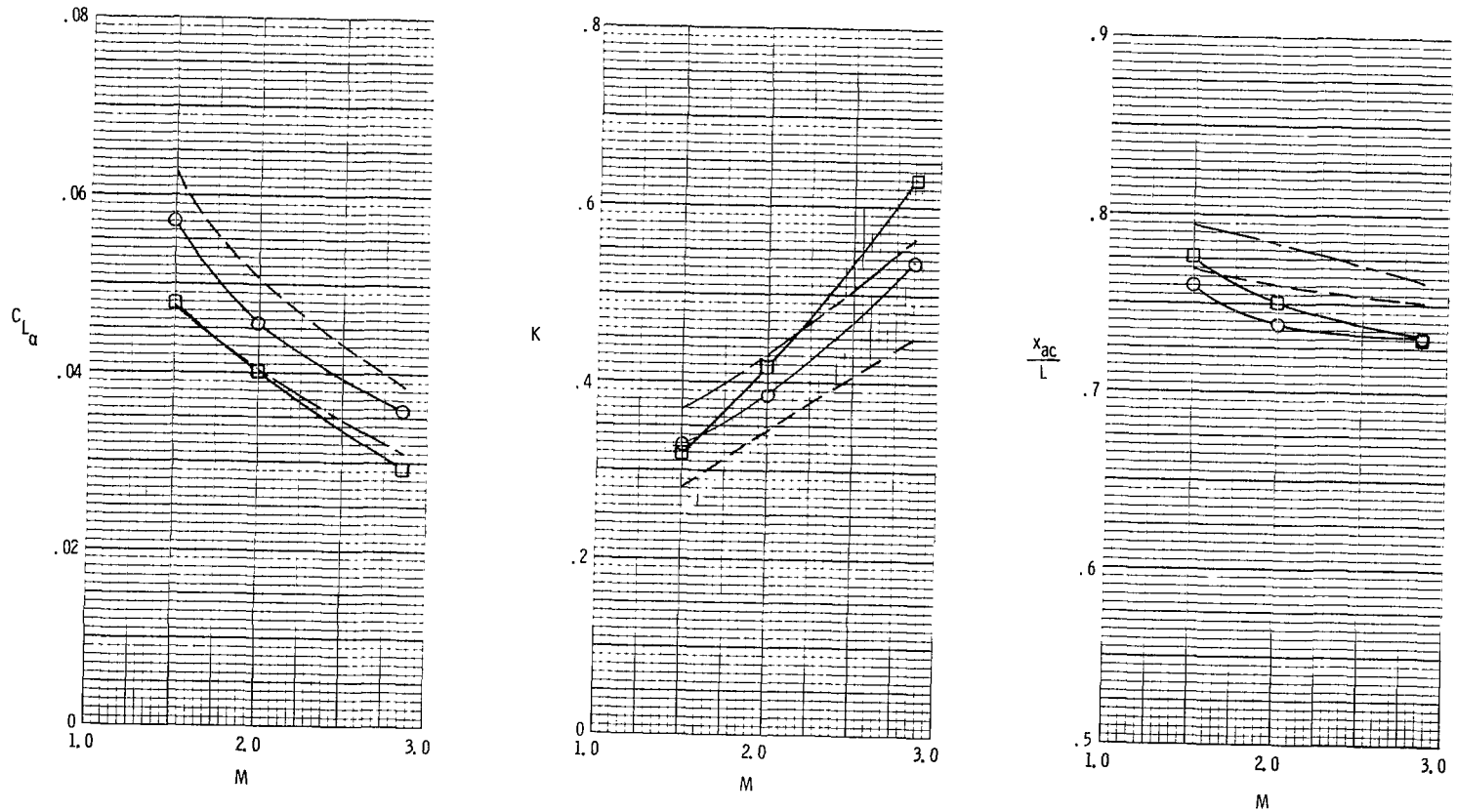

Figure 12.- Comparison of supersonic lifting surface theory with experiment.
$\alpha = 4°$.

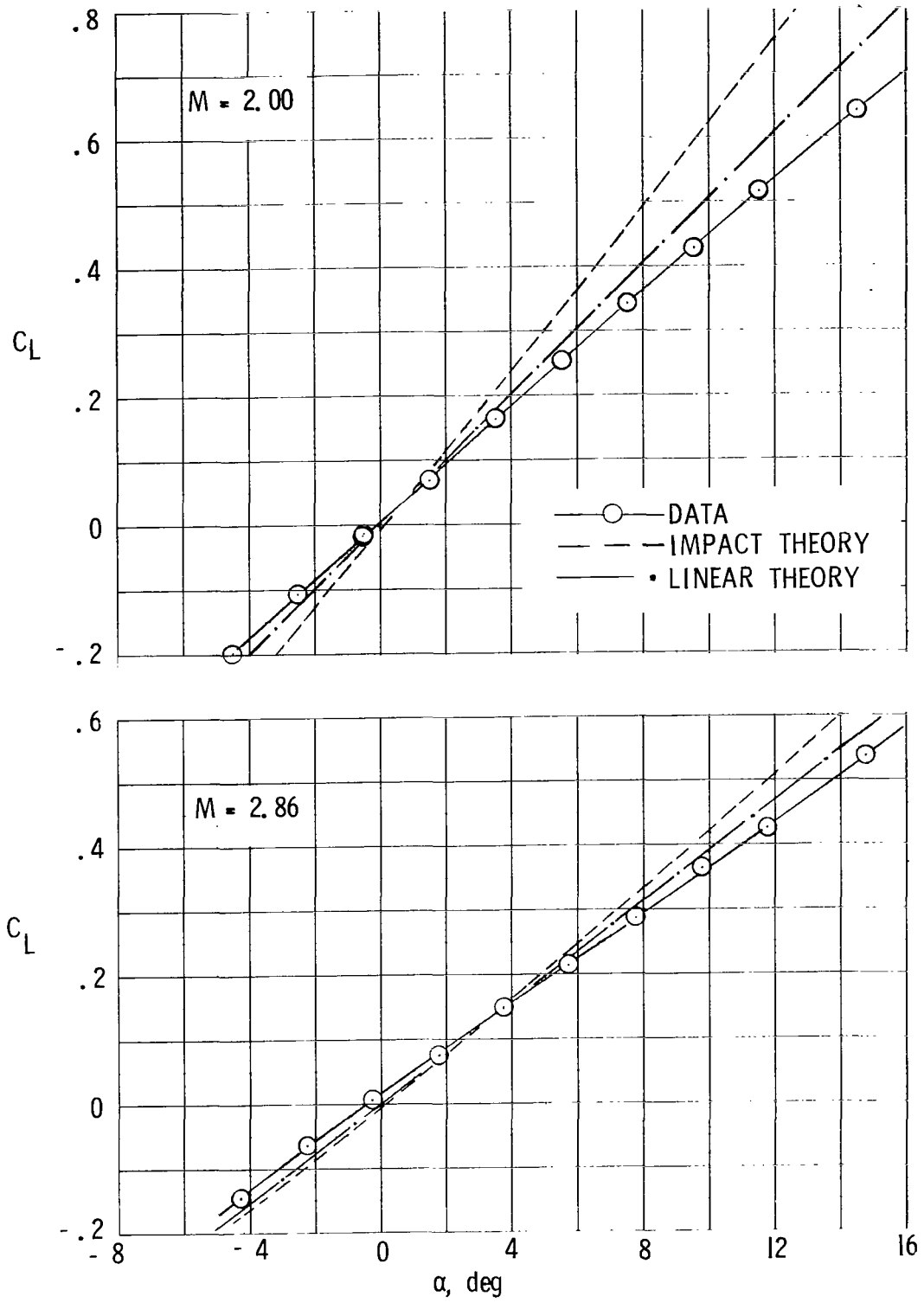

(a) Lift coefficient.

Figure 13.- Comparison of data with linear theory and impact theory for O(B+W+S)LW + B(P+W+S)IN configuration.

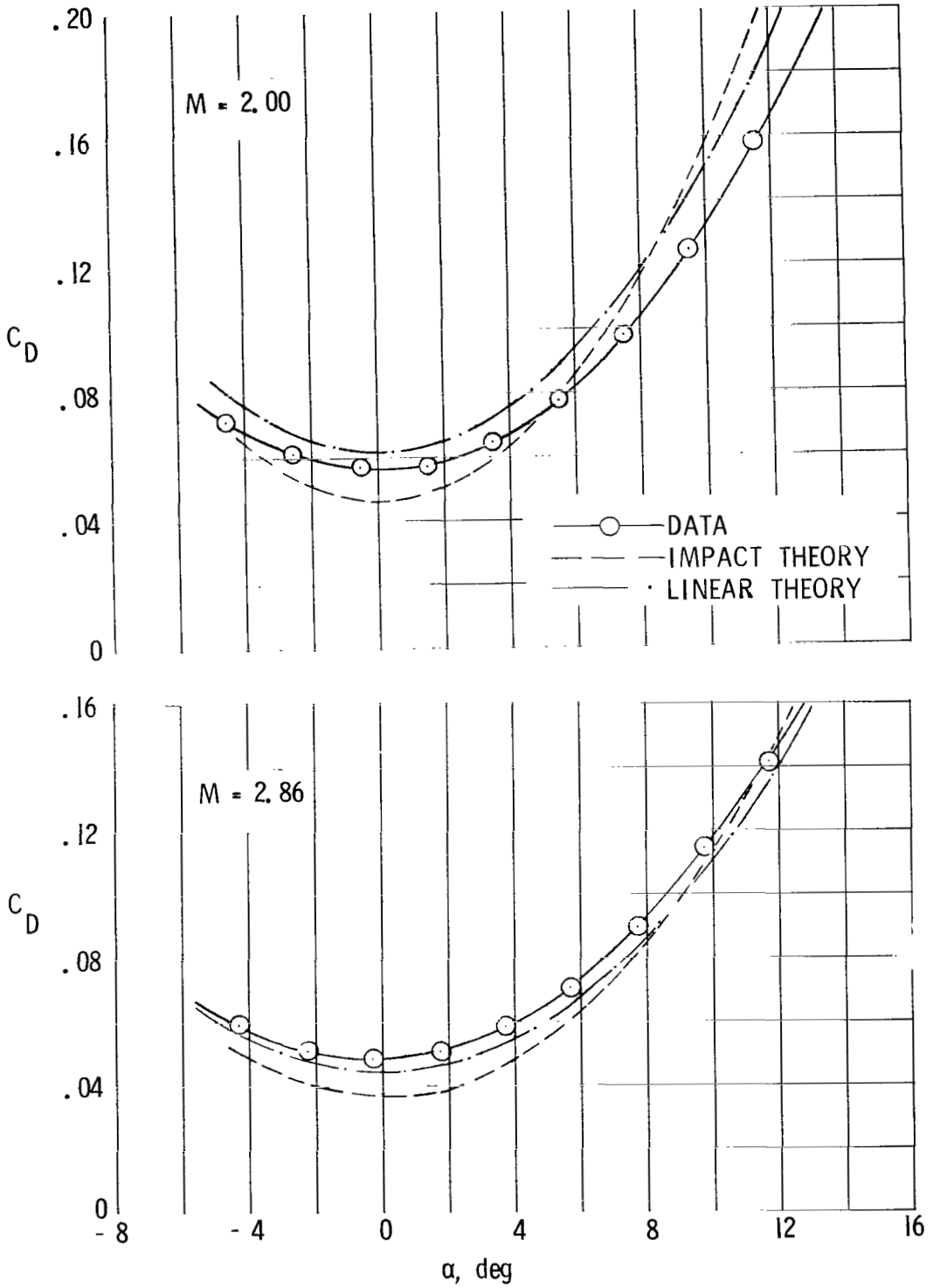

(b) Drag coefficient.

Figure 13.- Continued.

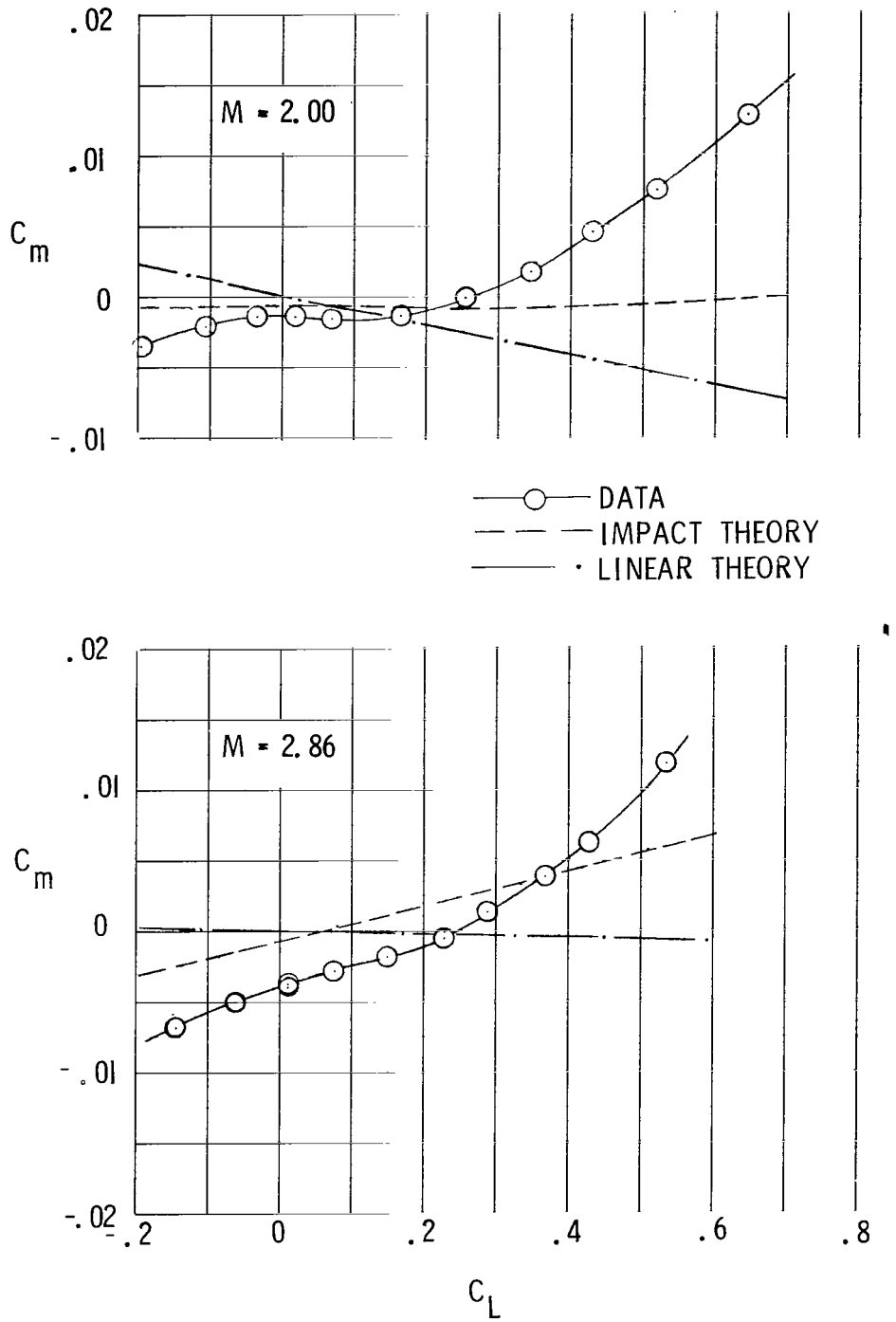

(c) Moment coefficient.

Figure 13.- Concluded.

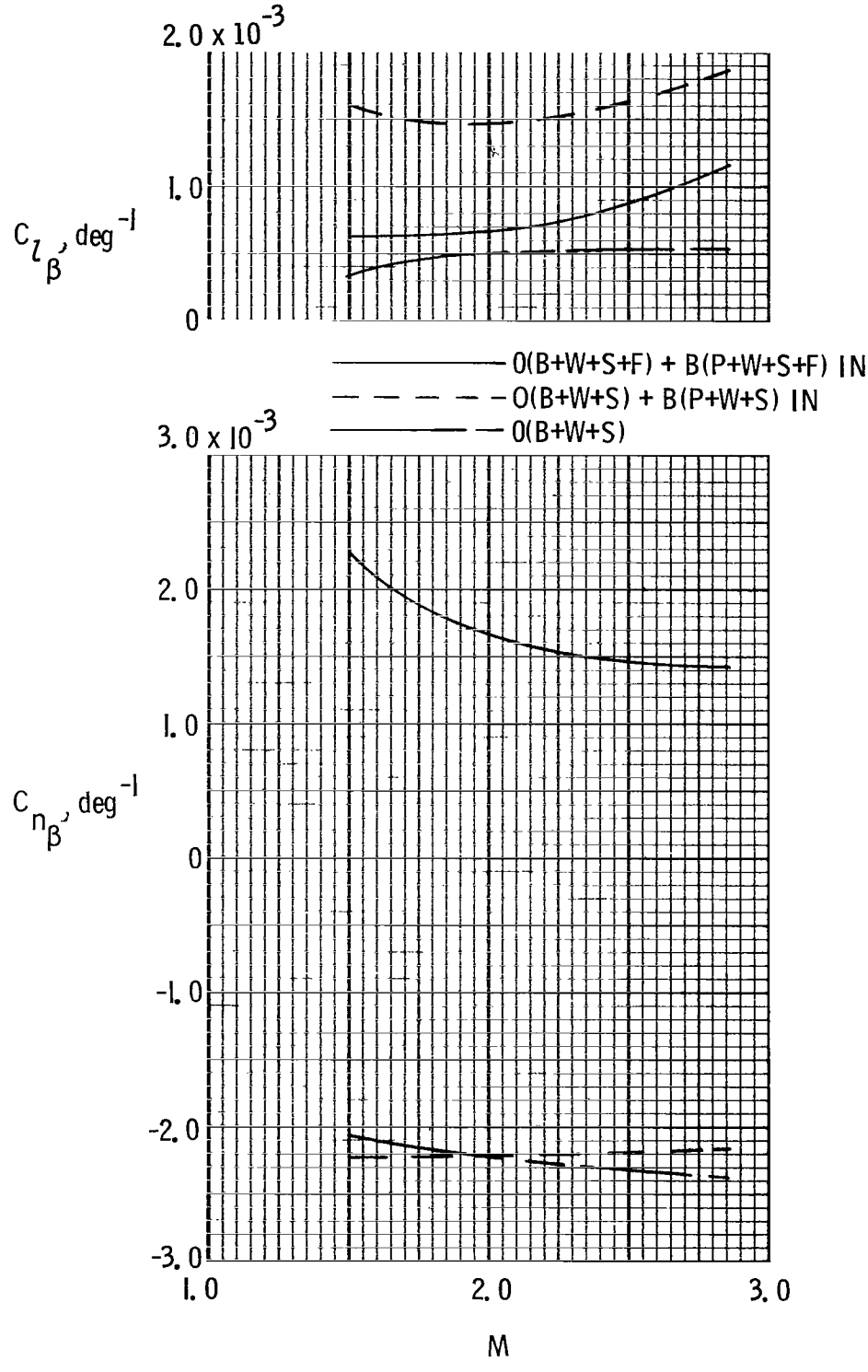

Figure 14.- Lateral-directional experimental characteristics of configuration buildup. $\alpha = 0°$.

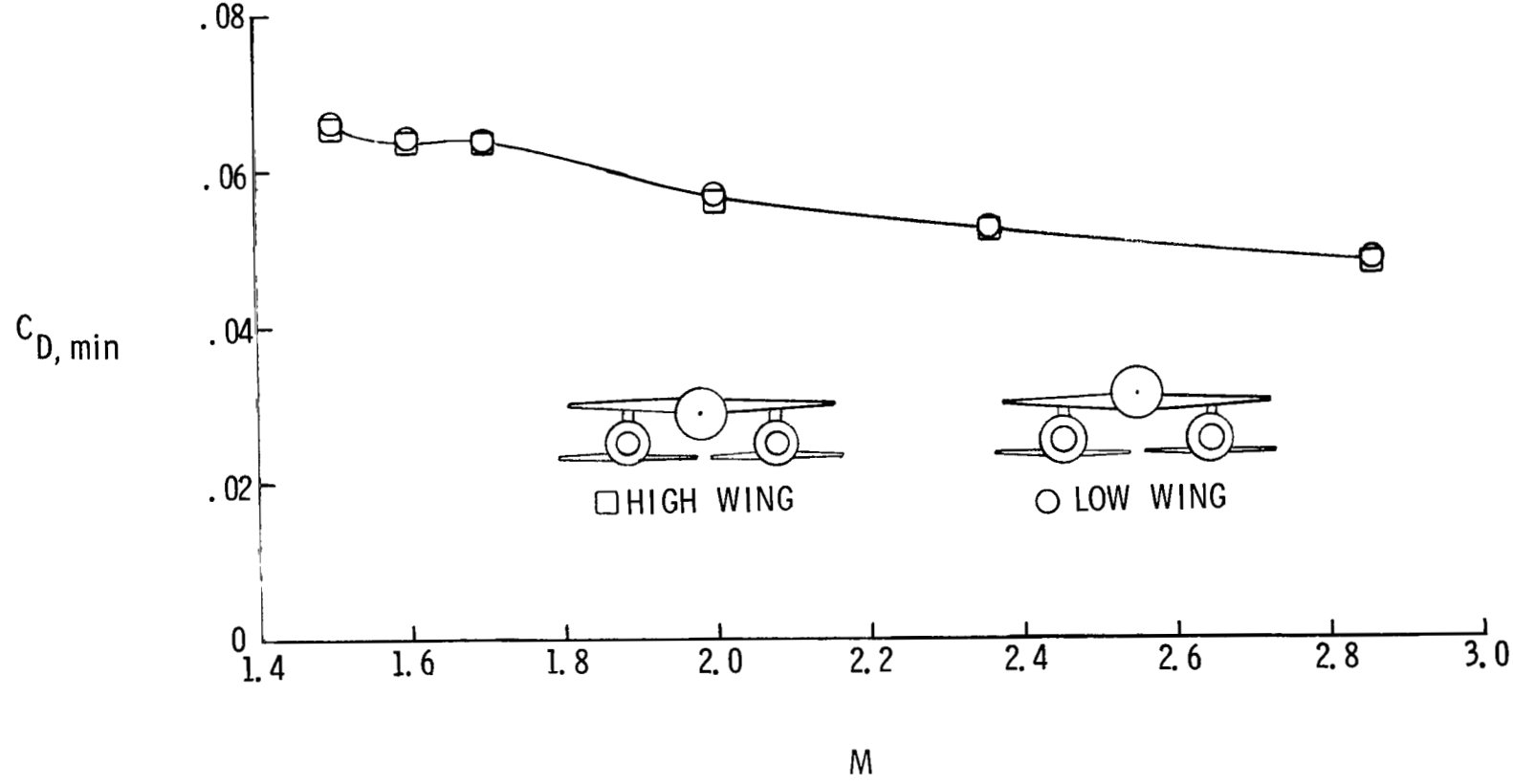

Figure 15.- Effect on minimum drag of orbiter wing position.

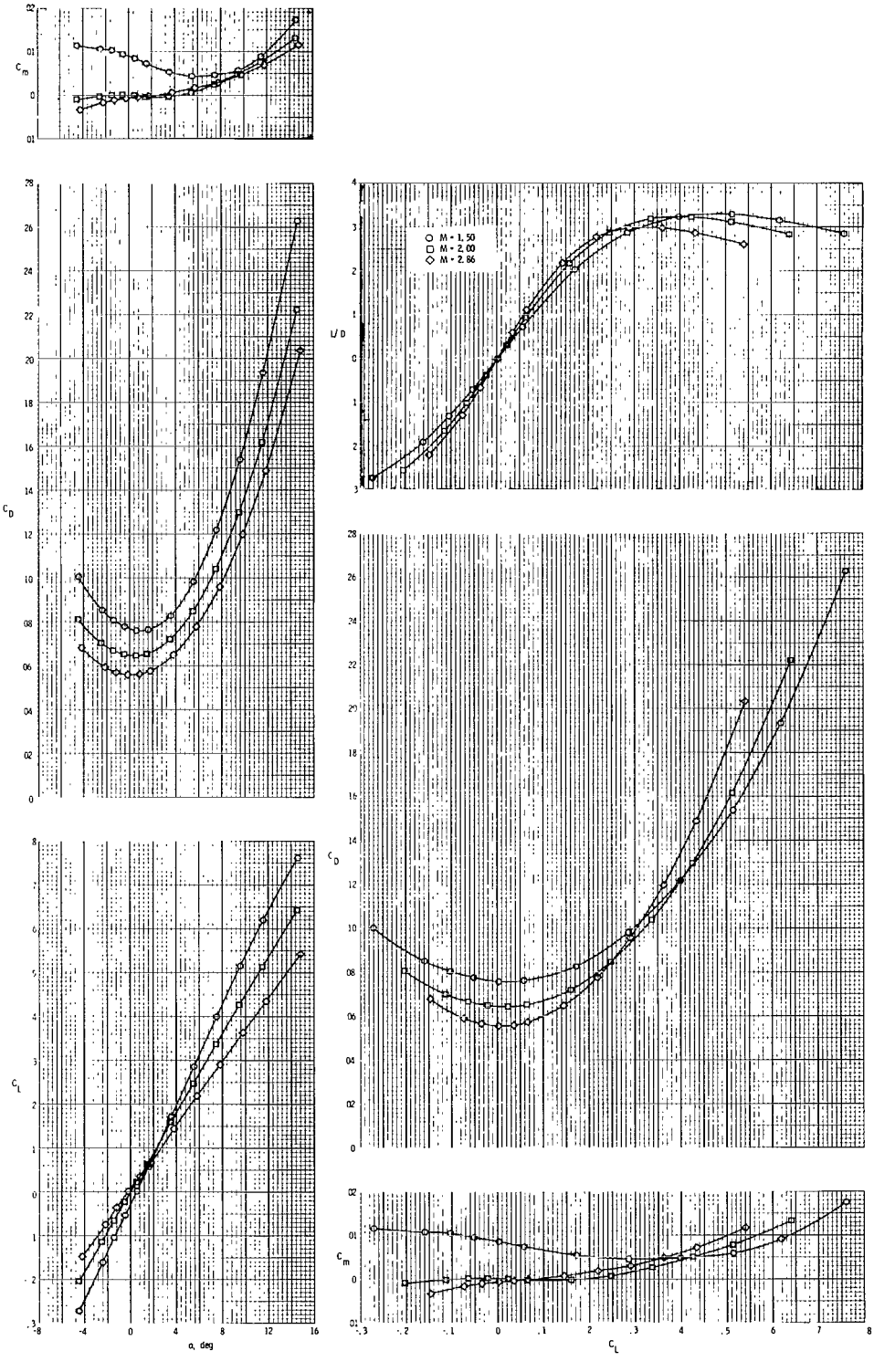

Figure 16.- Experimental aerodynamics at $\beta = 0°$ for O(B+W+S+F)LW + B(P+W+S+F)IN configuration.

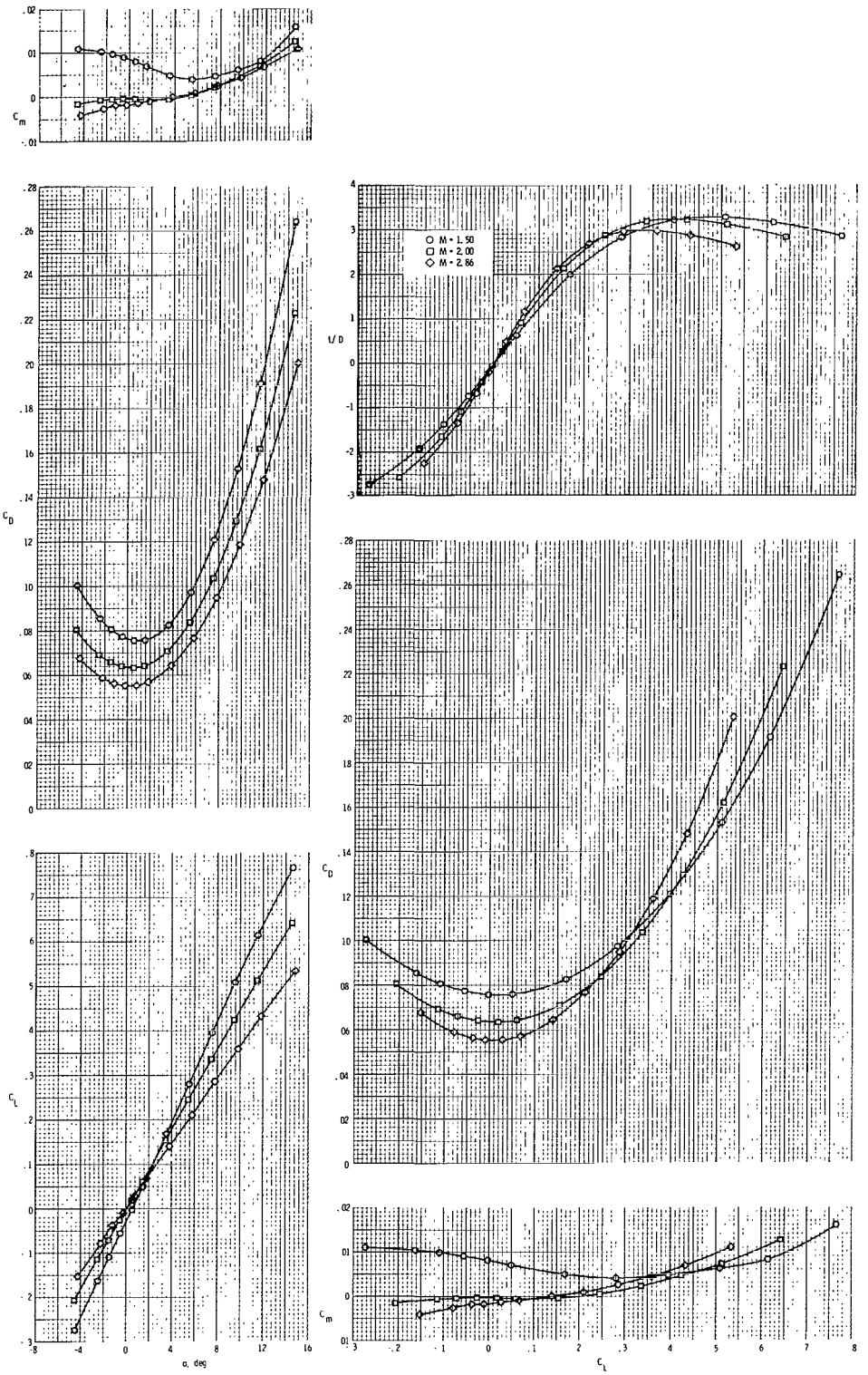

Figure 17.- Experimental aerodynamics at $\beta = 3°$ for O(B+W+S+F)LW + B(P+W+S+F)IN configuration.

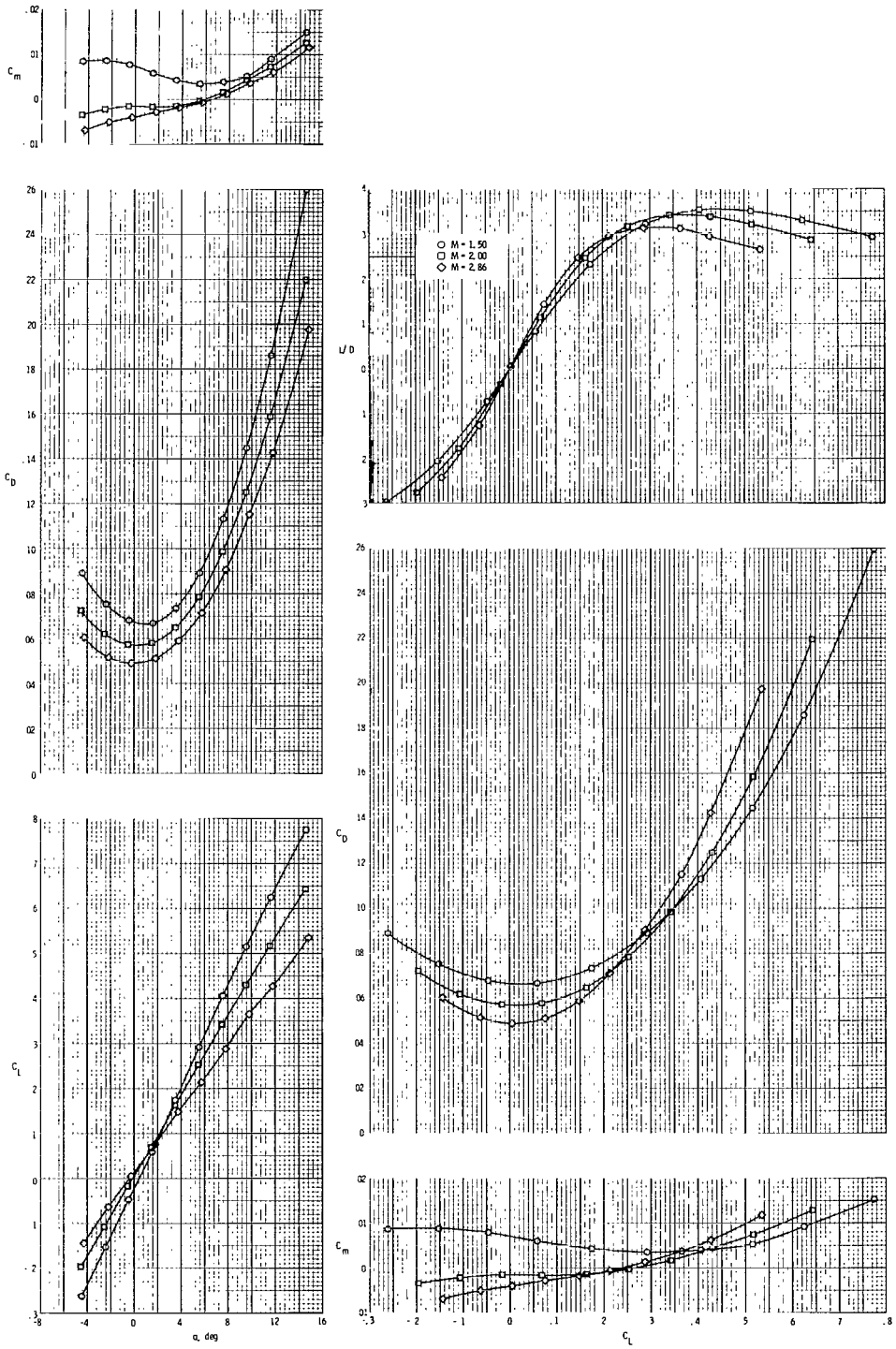

Figure 18.- Experimental aerodynamics at $\beta = 0°$ for O(B+W+S)LW + B(P+W+S)IN configuration.

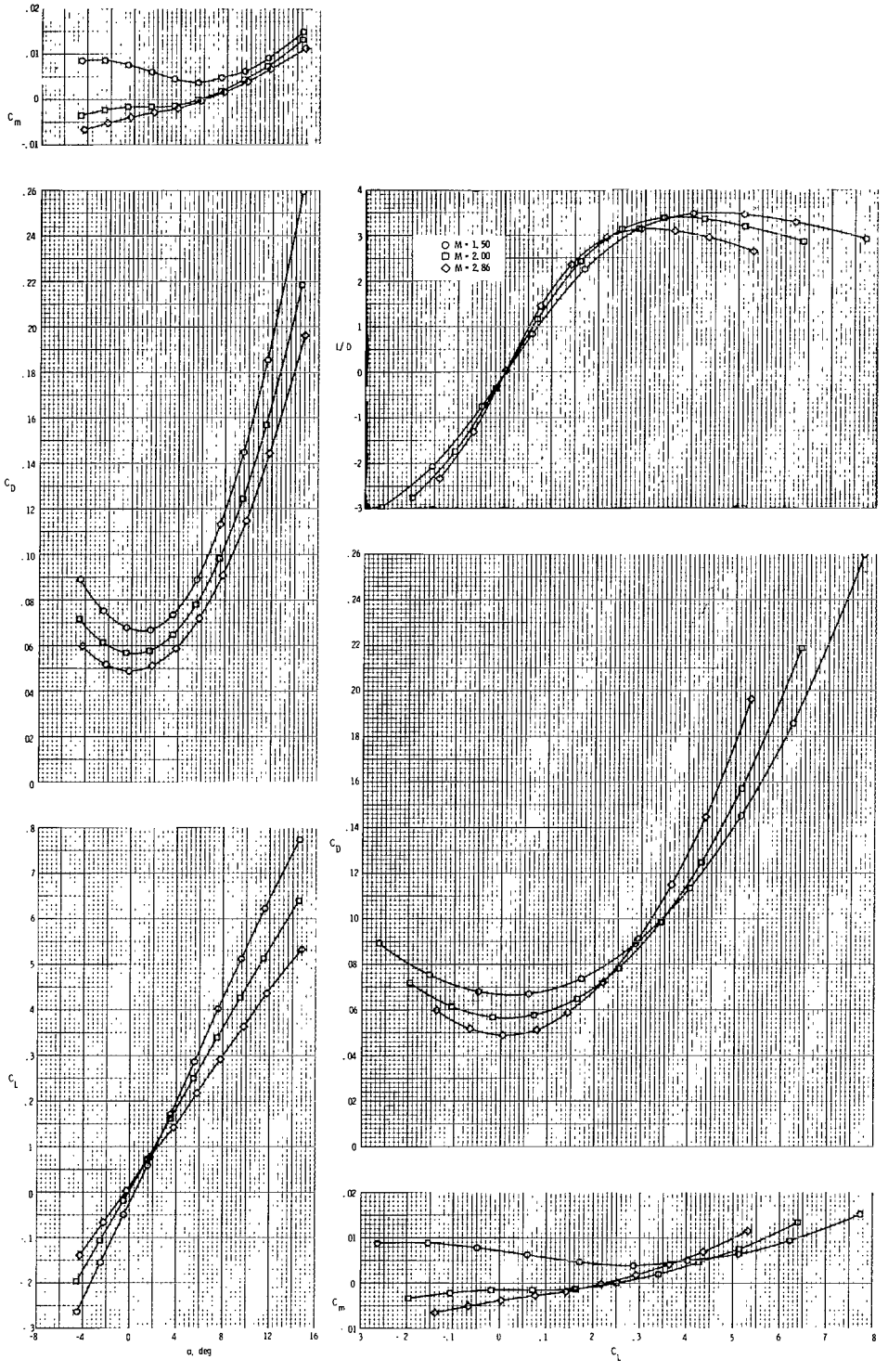

Figure 19.- Experimental aerodynamics at $\beta = 3°$ for O(B+W+S)LW + B(P+W+S)IN configuration.

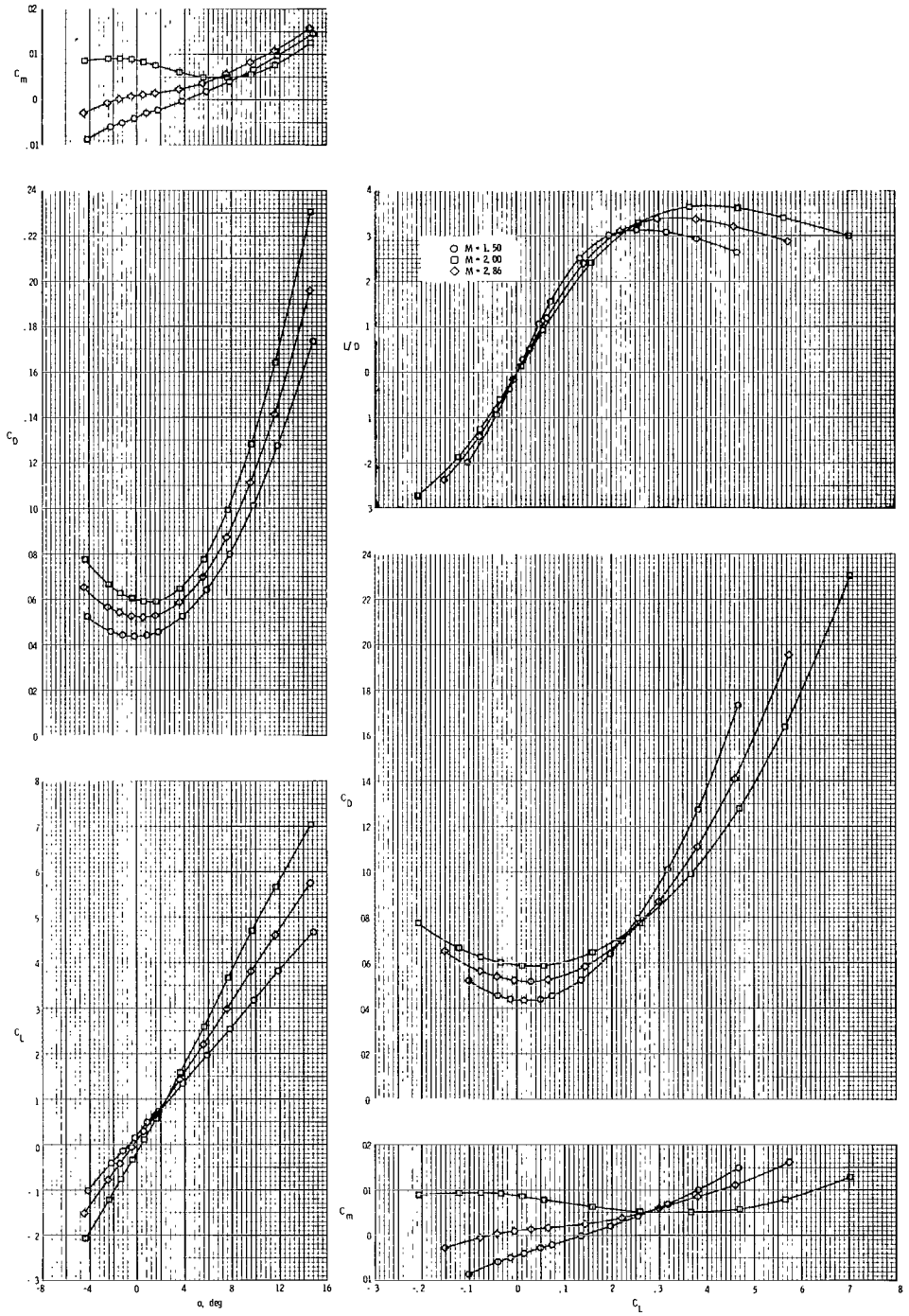

Figure 20.- Experimental aerodynamics at $\beta = 0°$ for O(B+W+S)LW + B(P)IN configuration.

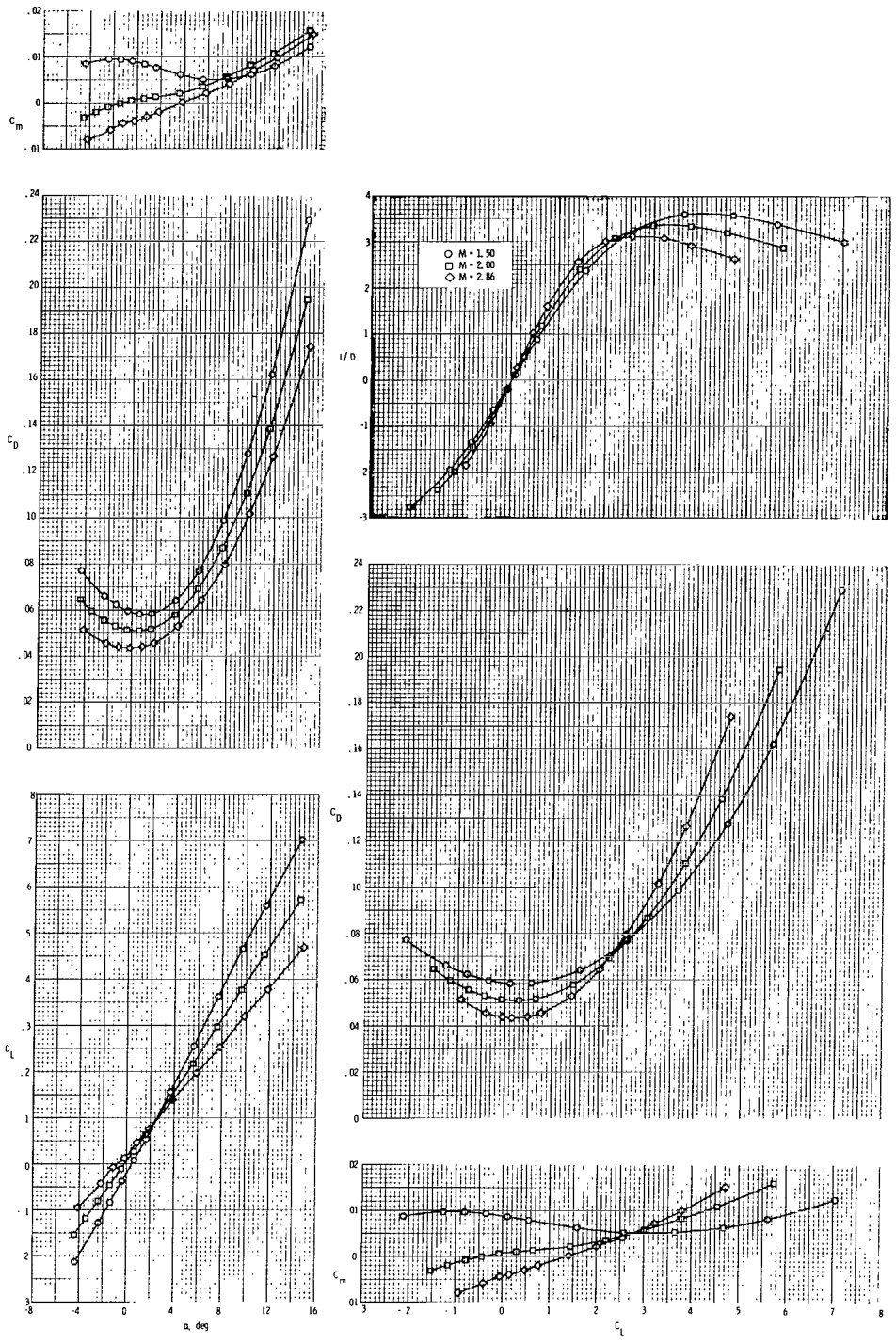

Figure 21.- Experimental aerodynamics at $\beta = 3°$ for O(B+W+S)LW + B(P)IN configuration.

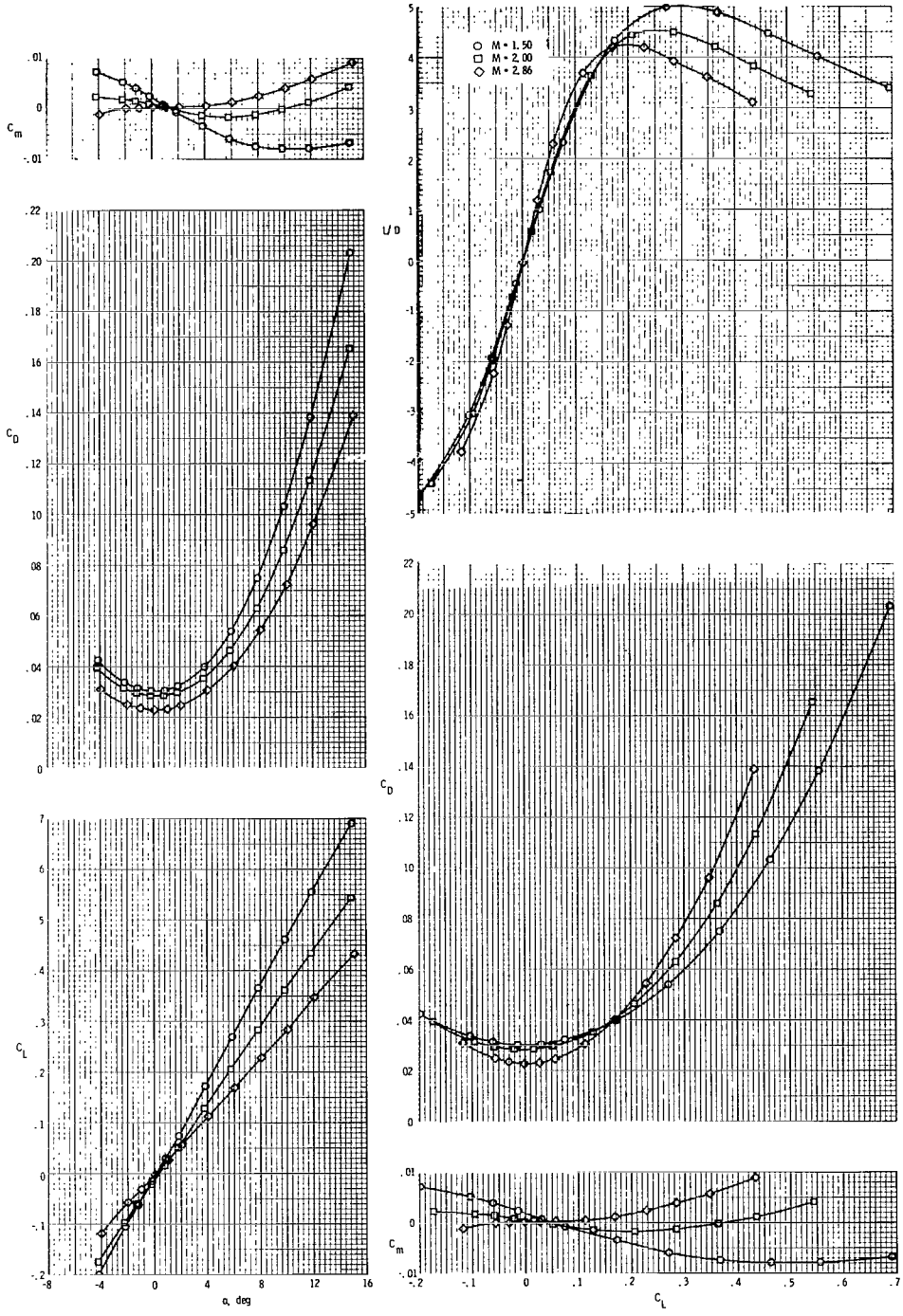

Figure 22.- Experimental aerodynamics at $\beta = 0°$ for O(B+W+S)LW configuration.

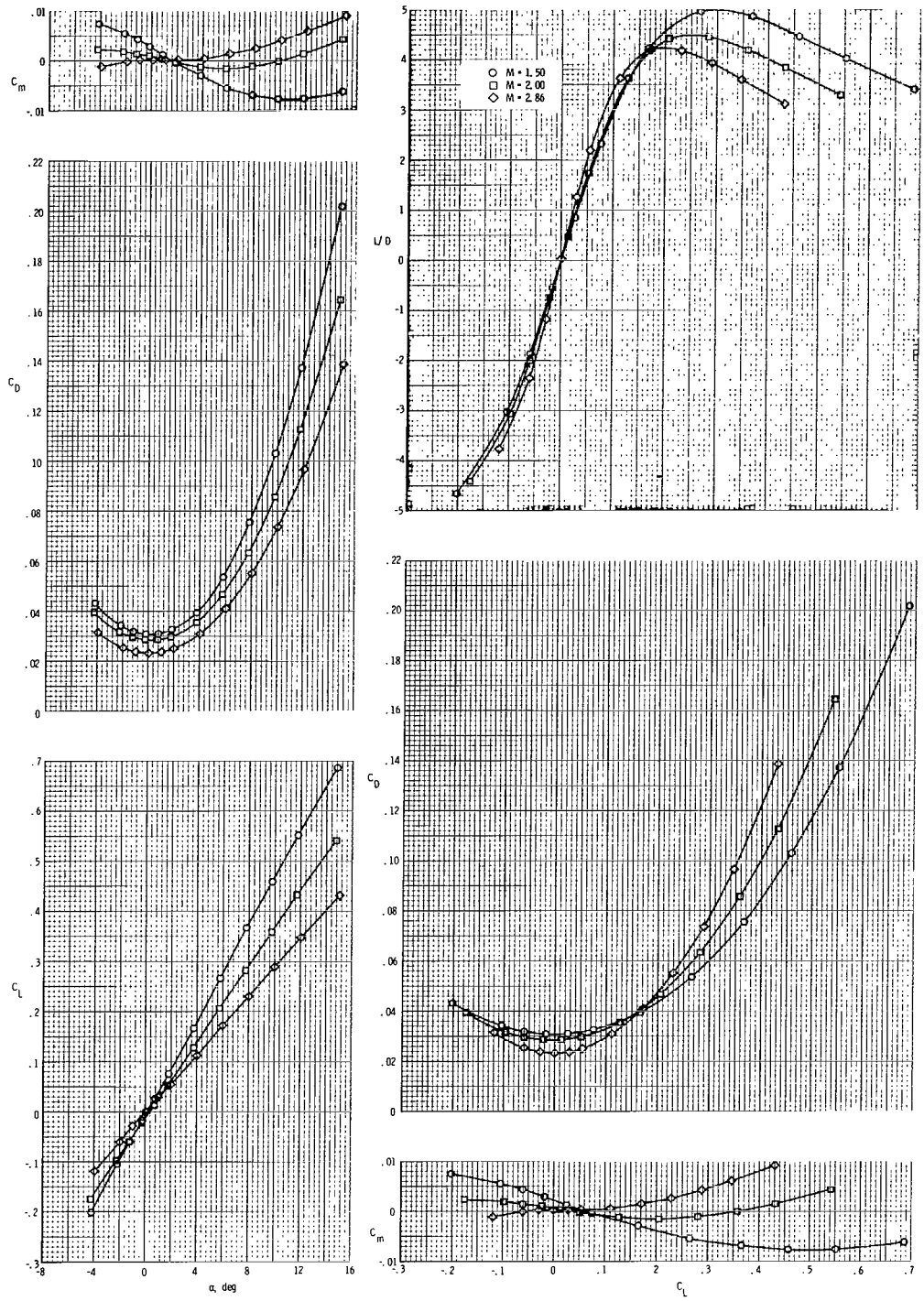

Figure 23.- Experimental aerodynamics at $\beta = 3°$ for O(B+W+S)LW configuration.

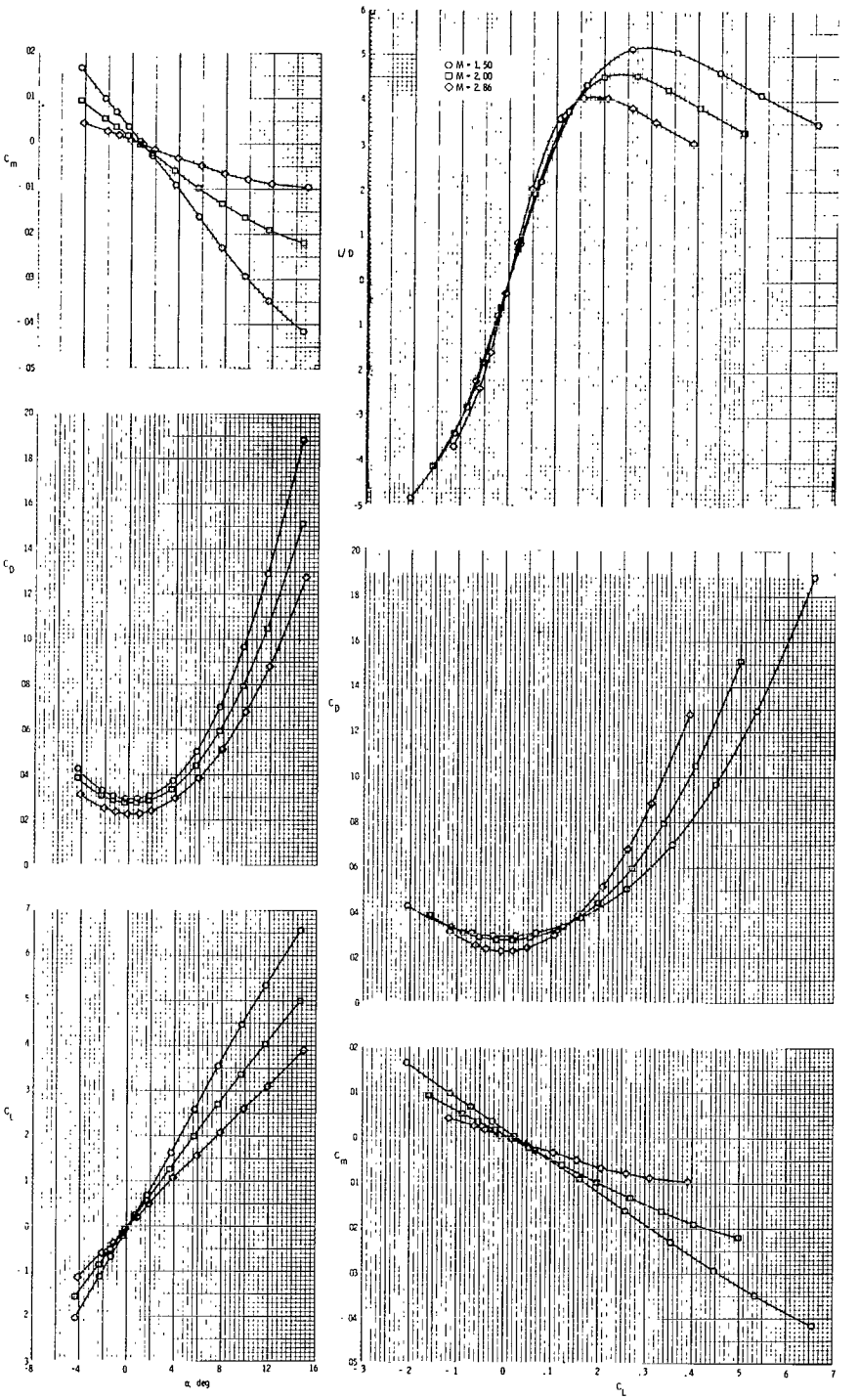

Figure 24.- Experimental aerodynamics at $\beta = 0°$ for O(B+W)LW configuration.

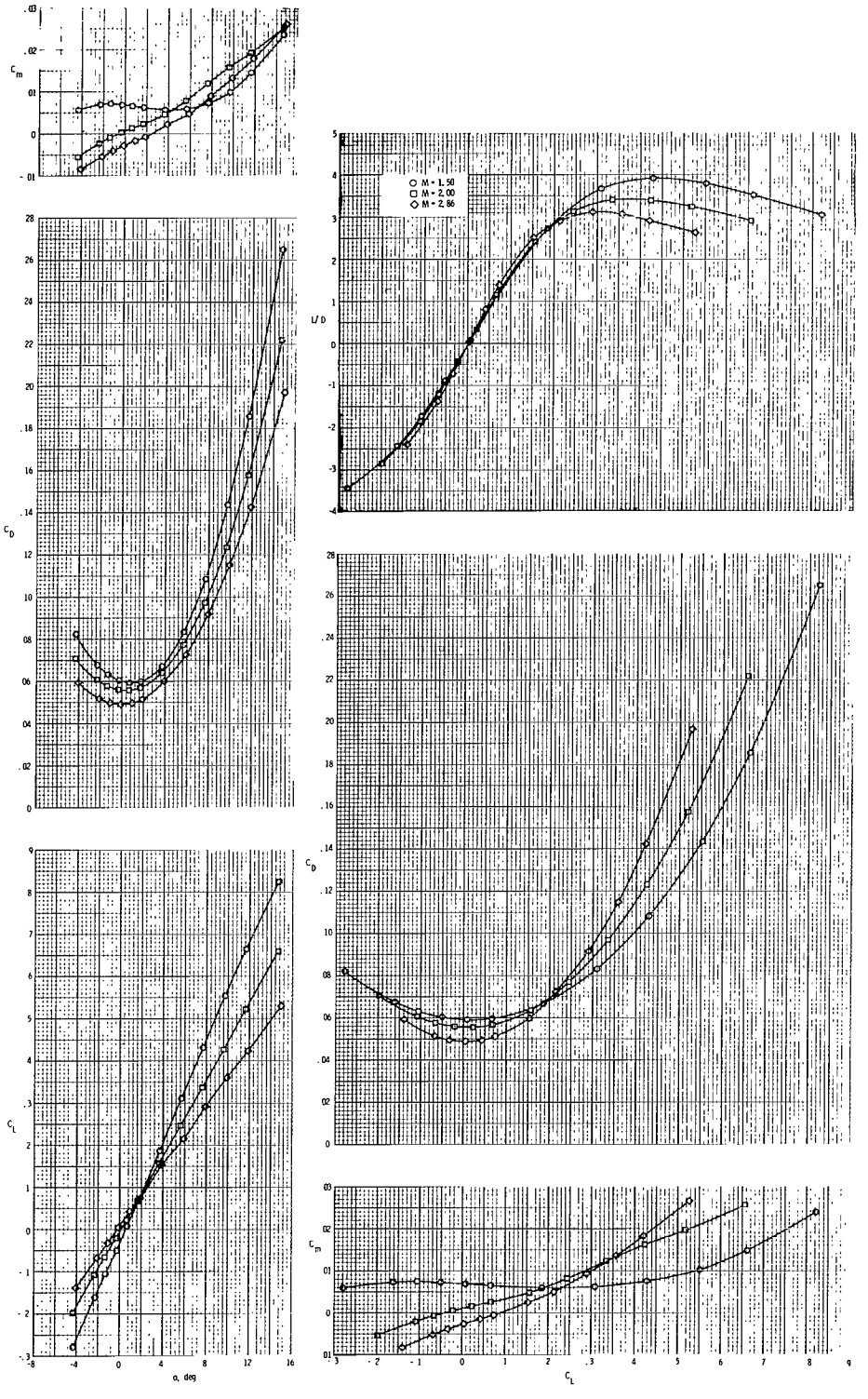

Figure 25.- Experimental aerodynamics at $\beta = 0°$ for 0(B+W+S)LW + B(P+W+S)IF configuration.

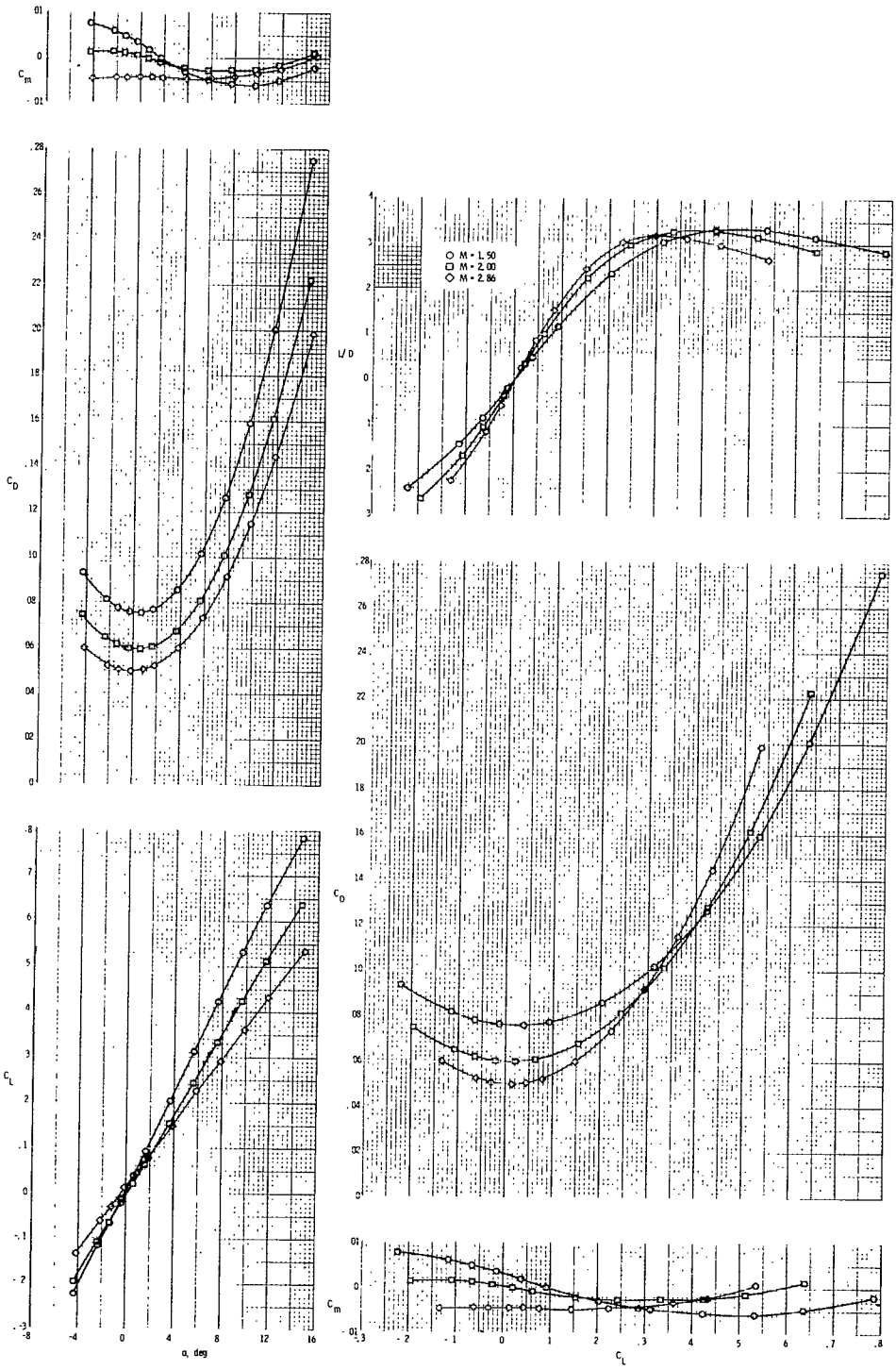

Figure 26.- Experimental aerodynamics at $\beta = 0°$ for O(B+W+S)LW + B(P+W+S)IA configuration.

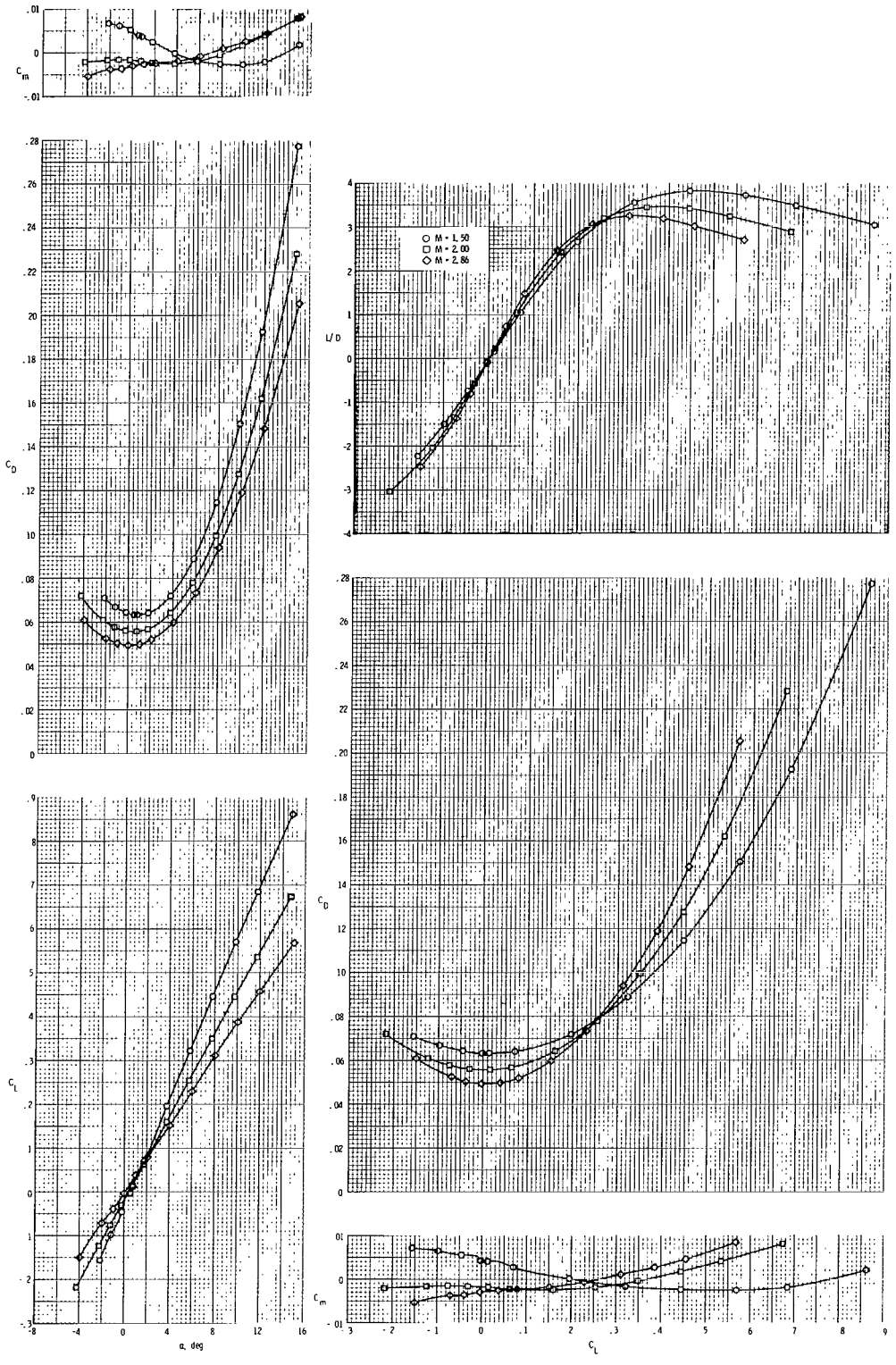

Figure 27.- Experimental aerodynamics at $\beta = 0°$ for 0(B+W+S)LW + B(P+W+S)ON configuration.

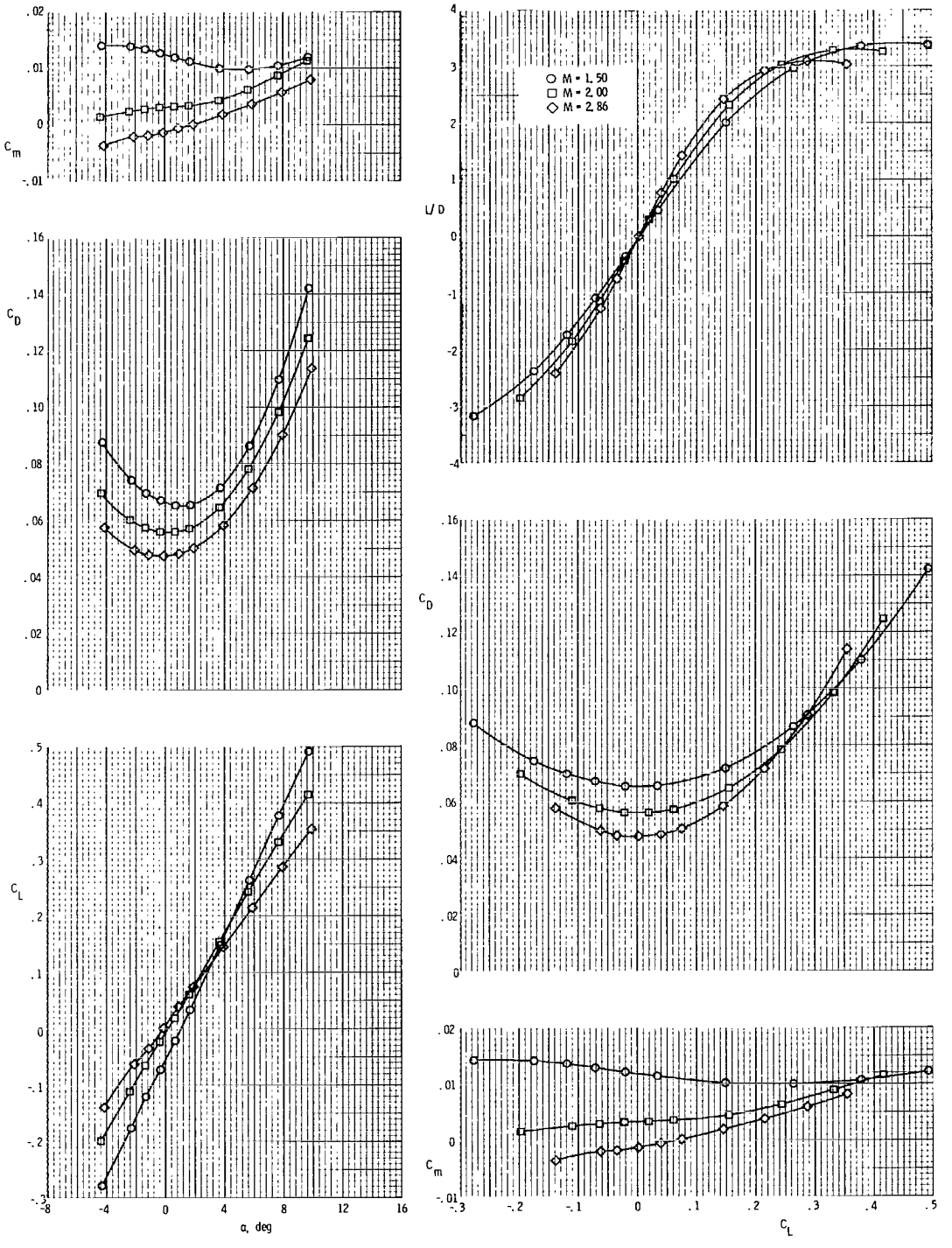

Figure 28.- Experimental aerodynamics at $\beta = 0°$ for O(B+W+S)HW + B(P+W+S)IN configuration.

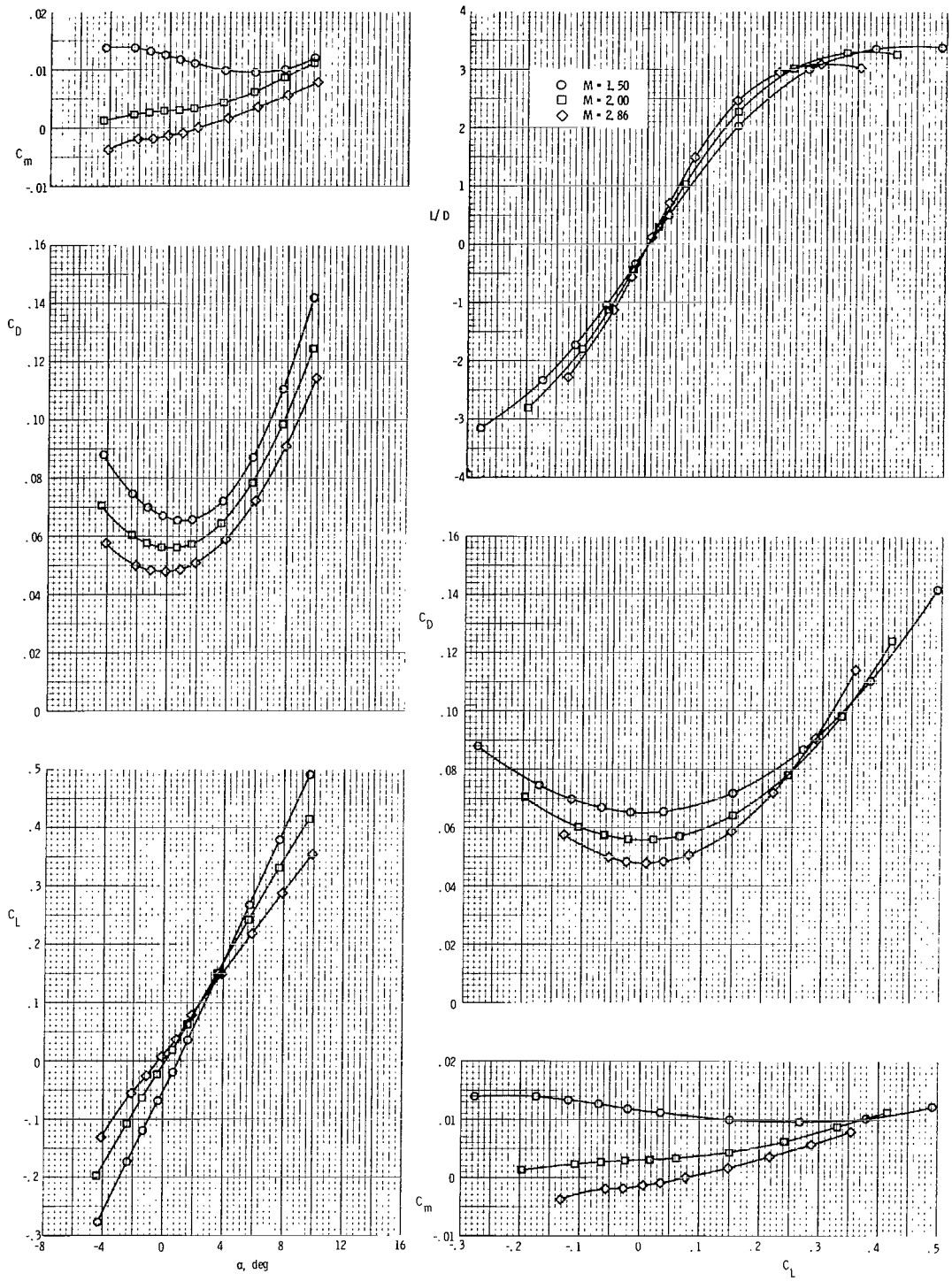

Figure 29.- Experimental aerodynamics at $\beta = 3°$ for O(B+W+S)HW + B(P+W+S)IN configuration.

1. Report No.	2. Government Accession No.	3. Recipient's Catalog No.
NASA TP-1888		

4. Title and Subtitle
AERODYNAMIC TESTS AND ANALYSIS OF A TURBOJET-BOOSTED LAUNCH VEHICLE CONCEPT (SPACEJET) OVER A MACH NUMBER RANGE OF 1.50 TO 2.86

5. Report Date
July 1981

6. Performing Organization Code
505-31-73-01

7. Author(s)
Gregory D. Riebe, William J. Small, and Odell A. Morris

8. Performing Organization Report No.
L-14509

9. Performing Organization Name and Address
NASA Langley Research Center
Hampton, VA 23665

10. Work Unit No.

11. Contract or Grant No.

12. Sponsoring Agency Name and Address
National Aeronautics and Space Administration
Washington, DC 20546

13. Type of Report and Period Covered
Technical Paper

14. Sponsoring Agency Code

15. Supplementary Notes

16. Abstract

Results from analytical and experimental studies of the aerodynamic characteristics of a turbojet-boosted launch vehicle concept through a Mach number range of 1.50 to 2.86 are presented. The vehicle consists of a winged orbiter utilizing an area-ruled axisymmetric body and two winged turbojet boosters mounted underneath the orbiter wing. This study concentrated primarily on drag characteristics near zero lift. Force measurements and flow visualization techniques were employed. Estimates from wave drag theory, supersonic lifting surface theory, and impact theory are compared with data and indicate the ability of these theories to adequately predict the aerodynamic characteristics of the vehicle. Despite the existence of multiple wings and bodies in close proximity to each other, no large scale effects of boundary-layer separation on drag or lift could be discerned. Total drag levels were, however, sensitive to booster locations.

17. Key Words (Suggested by Author(s))	18. Distribution Statement
Winged orbiter Horizontal take-off Supersonic aerodynamics Air-breathing booster	Unclassified - Unlimited Subject Category 02

19. Security Classif. (of this report)	20. Security Classif. (of this page)	21. No. of Pages	22. Price
Unclassified	Unclassified	53	A04

For sale by the National Technical Information Service, Springfield, Virginia 22161

NASA-Langley, 1981

National Aeronautics and
Space Administration

Washington, D.C.
20546

Official Business
Penalty for Private Use, $300

THIRD-CLASS BULK RATE

Postage and Fees Paid
National Aeronautics and
Space Administration
NASA-451

3 1 1U,A, 081281 S00903DS
DEPT OF THE AIR FORCE
AF WEAPONS LABORATORY
ATTN: TECHNICAL LIBRARY (SUL)
KIRTLAND AFB NM 87117

NASA

POSTMASTER: If Undeliverable (Section 158 Postal Manual) Do Not Return